

A MATHEMATICAL MODEL FOR CALCULATING
MASS TRANSFER IN THE DIFFUSION
LAYER

By

SHANNON DUGAN

Bachelor of Science

Oklahoma State University

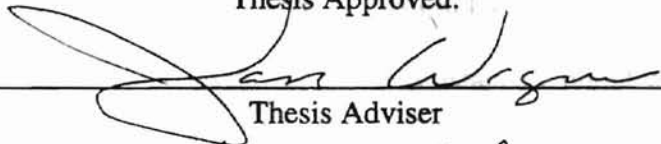
Stillwater, Oklahoma

1995

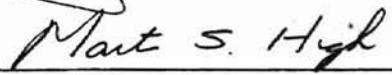
Submitted to the Faculty of the
Graduate College of the
Oklahoma State University
in partial fulfillment of
the requirements for
the Degree of
MASTER OF SCIENCE
May, 1999

A MATHEMATICAL MODEL FOR CALCULATING
MASS TRANSFER IN THE DIFFUSION
LAYER

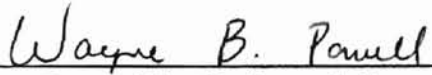
Thesis Approved:



Thesis Adviser







Dean of the Graduate College

ACKNOWLEDGMENTS

First and foremost, I would like to thank God for giving me the opportunity to enrich my life through this program and without whose grace I would not be where I am today.

I wish to thank those who have helped me, both directly and indirectly, to successfully complete this Masters program. I would like to thank Dr. Jan Wagner, my adviser, for his valuable guidance, and technical assistance without which this work might not have been possible. I would also like to thank Dr. Martin S. High and Dr. D. Alan Tree for their guidance throughout the program.

This project was sponsored by the Downhole Corrosion Consortium whose members are: Amoco, Conoco, GRI, Oryx and Phillips. I wish to thank all the sponsors for their support.

I would also like to thank my husband, Brian, whose support, both emotionally and financially, is greatly treasured. I would also like to thank my parents and family for helping me maintain sanity throughout this last year.

TABLE OF CONTENTS

Chapter	
1. Introduction.....	1
1.1 The Difficulty of Predicting CO ₂ Corrosion	1
1.2 The Importance of Predicting CO ₂ Corrosion.....	3
1.3 The Present CO ₂ Corrosion Prediction Model.....	4
1.4 The Purpose of This Work.....	5
2. Literature Review.....	6
2.1 Electrochemical Reaction Mechanisms of CO ₂ Corrosion	6
2.2 Physical Model.....	7
2.3 Mass Transfer Models.....	8
3. Diffusion Layer Modeling	18
3.1 Existing Diffusion Layer Model in DREAM.....	18
3.2 Proposed Diffusion Layer Model Development.....	22
3.3 Determination of Boundary Conditions.....	26
3.4 Comparison of Boundary Conditions for Reactive Species	30
4. Results.....	36
4.1 Comparison of Corrosion Rates.....	36
5. Conclusions and Recommendations	44
5.1 Conclusions.....	44
5.2 Recommendations.....	45
References.....	47
Appendix.....	50

LIST OF TABLES

Table 1. Well Specifications for Case 1.....	37
Table 2. Well Specifications for Case 2.....	39
Table 3. Well Specifications for Case 3.....	40
Table 4. Comparison of Corrosion Rate Predictions	43

LIST OF FIGURES

Figure 1. Composite Structure of Corrosion Processes for Annular Two-Phase Flow.	9
Figure 2. Fe^{++} Concentration vs. Normalized Diffusion Layer	
Thickness for de Waard and Milliams Method.....	31
Figure 3. HCO_3^- Concentration vs. Normalized Diffusion Layer	
Thickness for the de Waard and Milliams Method	32
Figure 4. Fe^{++} Concentration vs. Normalized Diffusion Layer	
Thickness for the Current Density Method.....	33
Figure 5. HCO_3^- Concentration vs. Normalized Diffusion Layer	
Thickness for the Current Density Method.....	34

NOMENCLATURE

b_a	anodic Tafel constant
b_k	cathodic Tafel constant
c_i	concentration of species i , moles cm^{-3}
D_i	diffusivity of species i , $\text{cm}^2 \text{s}^{-1}$
E_{corr}	corrosion potential, V
E_a	equilibrium potential of the anodic reaction, V
E_c	equilibrium potential of the cathodic reaction, V
F	Faraday's constant, 96500 C mol^{-1}
i_a	anodic corrosion current density, mA cm^{-2}
i_c	cathodic corrosion current density, mA cm^{-2}
i_i	current density of species i , mA cm^{-2}
I_a	metal-dissolution current, mA
I_{corr}	corrosion current, mA
J_i	flux of species i , $\text{mol cm}^{-2} \text{s}^{-1}$
N_i	flux density of species i , $\text{mol m}^{-2} \text{s}^{-1}$
P	partial pressure, kPa
Q	activation energy, $\text{J mol}^{-1} \text{K}^{-1}$
R	universal gas constant
R_i	reaction term, $\text{mol m}^{-2} \text{s}^{-1}$

t	temperature, °C
T	temperature, K
u_i	mobility of species i , mol Pa ⁻¹ m ⁻¹ s ⁻¹
v_i	fluid velocity, cm s ⁻¹
v	corrosion rate, mm yr ⁻¹
X	dimensionless length of diffusion layer
y^*	thickness of the diffusion layer, cm
z_i	charge of species i

Greek Symbols

α_a	anodic transfer coefficient
α_c	cathodic transfer coefficient
δ	thickness of the Nernst diffusion layer, cm
η_a	anodic overpotential, V
η_c	cathodic overpotential
Φ	electrostatic potential, V

Subscripts

δ	at the wall
o	at the turbulent-diffusion layer interface
avg	average value
ads	adsorbed

Chapter

bulk **bulk property**

1.0 The

Methods

results

2. Statistical

1990

1991/1992

1993/1994

Chapter 1

Introduction

1.1 The Difficulty of Predicting CO₂ Corrosion

The extent of CO₂ corrosion depends on the action of many parameters: temperature, pH, partial pressure of CO₂, water analysis, flow conditions, protective films, etc. Many experimental studies have been performed on the effect of individual parameters on CO₂ corrosion (de Waard and Milliams, 1975; Dugstad, 1994; de Waard and Lotz, 1993). On the basis of these studies, the effects of individual parameters are summarized as follows:

- pH — Increased pH lowers the solubility of FeCO₃, giving a higher probability for protective film formation. Higher pH also results in a lower corrosion rate because of the decreased availability of hydrogen ions.
- CO₂ — Higher CO₂ partial pressure increases the corrosion rate because the pH is reduced.
- Temperature — Higher temperature increases the corrosion rate because the electrochemical reactions are accelerated. However, precipitation rates also increase. Thus, protective films can form more easily at higher temperatures and can lower the corrosion rate.

- Protective films — FeCO_3 films are considered to be protective in many cases. They reduce the corrosion rate by limiting the transport of chemical species involved in the electrochemical reactions.
- Flow — Higher flow rates usually increase the corrosion rates by increasing the transport rates of reacting species to the metal surface by preventing or destroying protective films.

Beyond the diversity of environmental conditions, the CO_2 corrosion of steels is basically a very localized corrosion, which appears as pits and gutters of various sizes (Crolet, 1983).

For more than 50 years, laboratory experiments and theoretical models have been challenged to accurately represent general corrosion of steels by CO_2 in oil industry production waters (Trethewy, 1993). Except for extreme cases of erosion-corrosion, it appears that a corrosion product layer always covers bare metal surfaces after long exposures to aqueous CO_2 solutions. This observation is clear from field experience, but it is also probably true for laboratory experiments. If bare surfaces exist after short exposures, an increase in the duration of the exposure has always lead to an increased probability of observing corrosion product layers (Dugstad, 1992). Typically, exposures have never exceeded one month in laboratory tests (Dugstad, 1992). For example, corrosion by H_2S can take considerable time to develop and may go unnoticed in short-term laboratory tests (Greco and Wright, 1962). Therefore, the effect of time on CO_2 and H_2S corrosion must be recognized as a phenomenon in its own right, especially when extrapolating laboratory data to field data.

Field experience also reveals the protective behavior of certain corrosion product layers. This is not merely the absence of corrosivity in the medium, but an absence of corrosion under extremely aggressive conditions that typically cause rapid and deep attack immediately adjacent to the protected areas. During well-servicing operations, observations reveal that the real corrosivities are considerably lower than those measured in the laboratory (Crolet, 1993; Trethewy, 1993). Therefore, empirical correction factors reconcile experimentally found corrosion rates to the rates found in the field (de Waard and Lotz, 1993). In particular, most corrosion “prediction” equations work reasonably well when corrosion exists, however they fail when corrosion does not occur (Crolet, 1993).

1.2 The Importance of Predicting CO₂ Corrosion

The uniform corrosion rate of steel increases with increasing CO₂ concentration. Early literature (Bacon et al., 1943, Hackerman et al., 1949; Bilhartz et al., 1952; Greenwell, 1952) attributes this increase in corrosion rate to lowering of the solution pH with CO₂ addition. On the basis of correlations between field observations, studies carried out in the 1950's emphasized the effect of CO₂ partial pressure on the corrosivity of a well through the acidizing of the water phase by carbonic acid (Bacon et al., 1943; Bilhartz et al., 1952). While this decrease in pH is a significant factor, it has been shown that CO₂ has a more direct role in corrosion, and that corrosion rates are generally higher in CO₂ solutions than in solutions of completely dissociated acids of the same concentration (de Waard and Milliams, 1975).

At high CO₂ partial pressures, the uniform corrosion rates presented in much of the literature are extremely high. To combat these high corrosion rates, the use of alloyed production tubings has increased. However, the cost involved in placing alloyed tubings in all wells is not economically feasible (Timmins, 1996). For CO₂ corrosion in the oil and gas industry alone, the simple alternative between low alloy and stainless steels represents differences in investment costs of billions of dollars (Trethewy, 1993). Considering the significant cost associated with the replacement of corroded material, a method of predicting the corrosivity of a well is significant.

1.3 The Present CO₂ Corrosion Prediction Model

Empirical models, based on experimental studies (de Waard and Milliams, 1975; de Waard and Lotz, 1993; Nestic et al., 1995; Tewari and Campbell, 1979; Trethewy, 1993) are difficult to extrapolate and may have unrealistic limits that do not represent the full gamut of field conditions (de Waard and Milliams, 1975; de Waard and Lotz, 1993). These models have been the main tools used by industry to predict corrosion rates. However, they require a limited number of parameters such as partial pressure of CO₂, pH and temperature to calculate the corrosion rate. In addition, many of these models assume that mass transfer effects are negligible.

A deterministic mass transfer model of uniform CO₂ corrosion rates in downhole natural gas well environments, DREAM, has been developed for annular flow (Liu, 1993; Sundaram et al., 1996). This model is composed of recent work in chemistry, thermodynamics, mass transfer, and fluid flow. Recent research has been focused on the improvement of the thermodynamic and pressure drop correlations of this model

(Sundaram et al., 1996). Although model predictions of corrosion rates compare fairly well with caliper surveys obtained from wells with widely varying corrosion environments, the ability of the model to predict corrosion rates has been somewhat insensitive to improvements in these two areas. Therefore, a new approach to diffusion layer mass transfer modeling was taken.

1.4 The Purpose of This Work

The calculation of corrosion rates is dependent upon the temperature, pressure, amount of species diffusing to the surface, and the kinetic parameters at the surface. The primary purpose of this work is to:

- Survey previous work done on improvements to DREAM (Liu, 1991; Sundaram, 1996).
- Evaluate the current mass transfer model in DREAM and determine the deficiencies of the model.
- Compare empirical formulations (de Waard and Milliams, 1975; de Waard and Lotz, 1993; Nesic et al., 1995; Tewari and Campbell, 1979; Trethewy, 1993) to those relying on fundamental principles and incorporate the best available correlation into DREAM.
- Ensure that the reactions of the active species at the wall are taken into account in the diffusion layer model.

Chapter 2

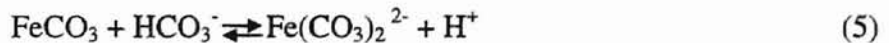
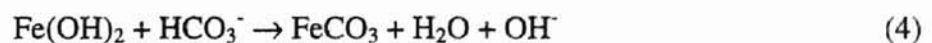
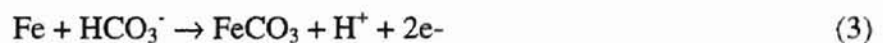
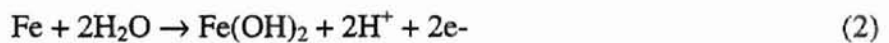
Literature Review

2.1 Electrochemical Reaction Mechanisms of CO₂ Corrosion

The uniform corrosion of iron exposed to CO₂ dissolved in water proceeds by coupled electrochemical reactions. When no solid reaction products are formed, the overall anodic dissolution reaction can be written as:



This reaction appears to proceed through intermediates involving hydroxyl ions (OH⁻) in such a way that the rate of anodic dissolution decreases with decreasing pH from pH 5 to pH 1 (Weickowski and Gahli, 1983). For example, Davies and Burstein (1980) proposed the following mechanism for the anodic dissolution of iron:



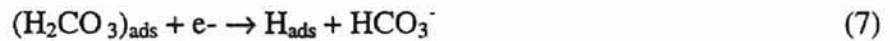
The rate determining step is the hydrogen evolution reaction, Equation 3.

The usual cathodic reaction is hydrogen evolution as expressed as:

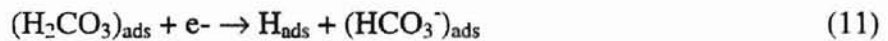


The increase in the rate of this reaction with decreasing pH more than offsets the pH dependence of the reaction in Equation 1 (Weickowski and Gahli, 1983), and the net effect is that corrosion rates decrease with increasing pH from pH 4 to pH 6.

Carbon dioxide primarily affects the cathodic reaction rate. Since hydrogen evolution is rate limiting, de Waard and Milliams (1975) proposed that hydrogen evolution could occur directly from carbonic acid as follows:



Whereas Schmitt and Rothmann (1984) proposed a non-electrochemical reaction mechanism with the rate determined by, Reaction 10:



Hydrogen atom combination to H_2 can occur via conventional routes. The overall reaction is the same as Equation 6 and proceeds in two steps. For example, the Volmer-Heyrovsky mechanism can be applied to most metals (Gray et al., 1989):



where H_{ads} is adsorbed hydrogen on the surface. Since the hydrogen adsorbs to the surface before reacting, the adsorbed hydrogen can be said to “catalyze” the hydrogen evolution reaction.

2.2 Physical Model

The downhole system in a gas well can be physically described by examining the corrosion process as follows (Sundaram et al., 1996): Natural gas with or without formation water leaves the reservoir and enters the tubing at high temperature and pressure (see Figure 1). Water condensation may occur at some upper position in the well due to temperature and pressure gradients. Under most circumstances, gas flow rates are relatively high, and the flow regime is classified as annular, two phase flow. The corrosive gases, CO_2 and H_2S , solubilize and dissociate in the liquid film and are transported through the turbulent film layer to the diffusion layer. In this layer, the mass transfer is dominated by diffusion and ion migration. Reactive species and dissolved gases (HCO_3^- , HS^- , CO_2 , and H_2S) diffuse and migrate through the diffusion layer to the tubing wall. The reactive species and dissolved gases (HCO_3^- , HS^- , CO_2 , and H_2S) react with ferrous ions at the wall to form a corrosion product layer either through a direct formation reaction or through precipitation. This corrosion product layer remains attached to the wall forming a protective layer. Disruption of this protective layer can be caused by erosion and/or dissolution and is strongly influenced by the structure of fluid flow (Trethewy, 1993).

2.3 Mass Transfer Models

Processes in which mass transfer is enhanced by chemical reaction are frequently encountered in the process industry (Littel et al., 1991). The chemical reactions that can occur in such processes range from a single irreversible reaction to multiple parallel and consecutive reactions. Well-known examples are the amine gas-treating processes where

the acid gas components CO_2 and H_2S are consumed by a chemical reaction in the alkanolamine solution during the absorption step and subsequently released by the reverse reaction (Versteeg et al., 1989).

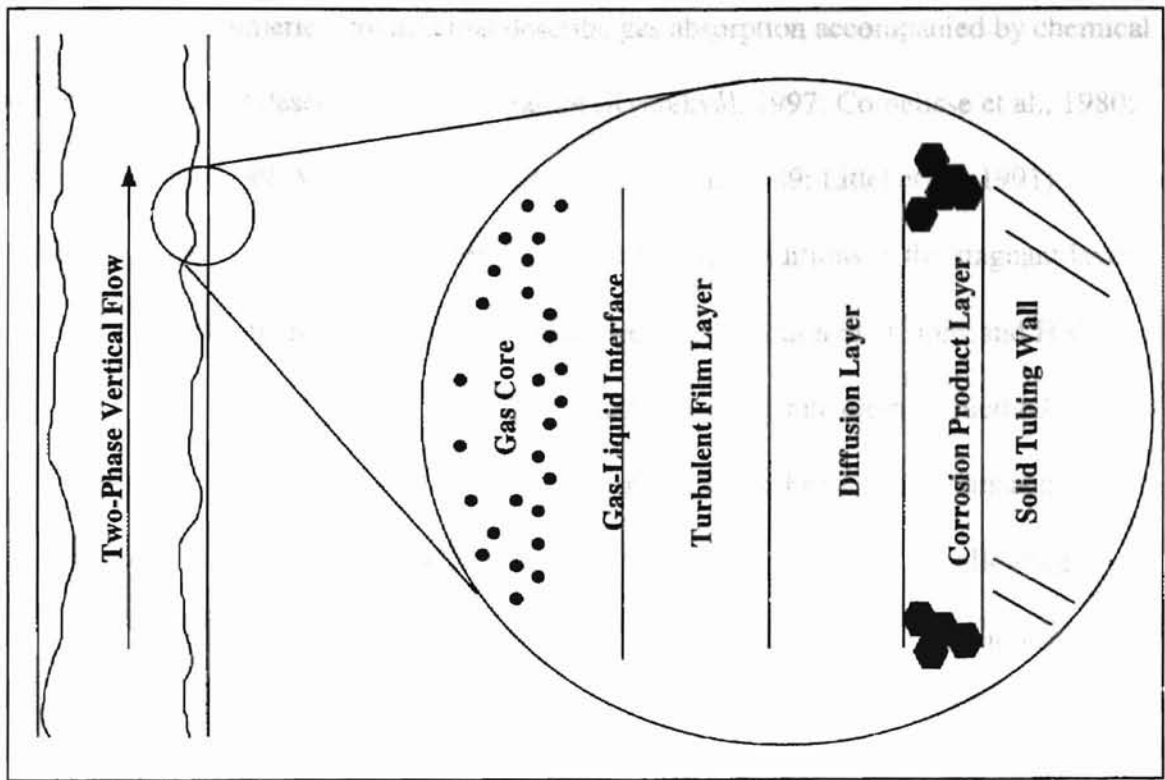


Figure 1. Composite Structure of Corrosion Processes for Annular Two-Phase Flow (Sundaram et al., 1996)

Several numerical models that describe gas absorption accompanied by chemical reaction have been described in the literature (Kvarekvål, 1997; Cornelisse et al., 1980; Versteeg et al., 1989; Versteeg et al., 1990; Bosch et al., 1989; Littel et al., 1991) .

Kvarekvål (1997) developed a model that simulates the conditions in the stagnant layer close to a dissolving iron surface, where heterogeneous reaction of H^+ ions and H_2CO_3 occurs. One-dimensional diffusion was calculated using a finite element method.

Homogeneous chemical reaction rates are determined from the rate constants and differential rate expressions. The assumptions of this model include the following:

- The cathodic rate of reaction is controlled by the transport of H^+ ions and carbonic acid.
- The flux of molecules is exclusively caused by diffusion.
- The diffusion is one-dimensional, and occurs only in the diffusion layer.
- Diffusion of each species involved (H^+ , H_2CO_3 , CO_2 , HCO_3^- , CO_3^{2-} , OH^- and Fe^{2+}) is independent of the others.

However, electroneutrality criteria are not strictly applied to each point in the diffusion layer; the presumed presence of a supporting electrolyte is assumed to depress the electric field set up by the diffusing ions. The mathematical method applied to this model was the sequential explicit space point method. Concentration changes caused by one-dimensional diffusion were calculated for all species by the following procedure:

- During the time Δt , the concentration of an arbitrary ion or molecule at the point i in the diffusion layer changes from c_i to c'_i .

$$c'_i = c_i + \Delta c_i \quad (14)$$

- The magnitude of the change is Δc_i , and depends on the concentrations of the particular species at the adjacent points $i-1$ and $i+1$.

$$\Delta c_i = \Delta t \cdot \frac{D}{h^2} (c_{i-1} - 2c_i + c_{i+1}) \quad (15)$$

where D is the diffusion coefficient of the specific ion or molecule and h is the distance of each step in the numerical method.

The model results are strongly dependent upon the time step for unsteady state predictions. If this time step is too large, the fast reactions are "degraded" to slower reactions, thereby, decreasing their weighted effect on the results. A large time step could also exaggerate the diffusion in the diffusion layer. This model overpredicted corrosion rates from 25% up to 250%. Consequently, the results of this model are purely theoretical "worst case" predictions for the given conditions.

Cornelisse et al. (1980) created a mass transfer model for a system involving the simultaneous transfer of two components from or to a medium where complex, reversible reactions take place. The specific application, represented in the following equations, was the simultaneous transfer of CO_2 and H_2S into and out of an amine solution.



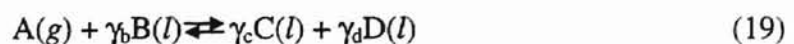
The kinetics of this system were obtained from the published literature:

$$R = k_2 \left([\text{CO}_2] [\text{R}_2\text{NH}] - \frac{1}{K_{\text{CO}_2}} \frac{[\text{R}_2\text{NCOO}^-] [\text{R}_2\text{NH}_2^+]}{[\text{R}_2\text{NH}]} \right) \quad (18)$$

where R is the rate of transfer of CO_2 into and out of an amine solution.

To reduce the number of parameters and variables, only overall reactions were considered. The stagnant film model described the mass transfer in the gas phase, as no reaction occurs in this region. Higbie's penetration theory (Bird et al., 1960) was applied to the liquid phase mass transfer. The model begins with total species balances and ends with a total acid balance that states that the accumulation of acid is equal to the net inflow by diffusion. This model, however is restricted to only a few stoichiometric schemes. One drawback to this approach is that the diffusivities of each species were averaged and a mean diffusivity was used. The mathematical treatment of this model is as follows: The equations are first transformed into dimensionless form and then discretized. A three-point backward-difference numerical scheme is then used to numerically solve for the mass transfer rates (Baker and Oliphant, 1960; Cornelisse et al., 1980). This numerical method is not only quite involved, but also introduces a large truncation error into the result (Versteeg et al., 1989). Therefore, the accuracy of this model is subject to the minimization of this truncation error.

Versteeg et al. (1989, 1990) presented a numerical model that describes the absorption of a gas accompanied by multiple parallel, reversible chemical reactions. Their objective to describe the absorption of CO₂ and H₂S in alkanolamine solutions laid the framework for the reaction schemes modeled. The reaction stoichiometry and the reaction rate expressions were of a generalized form:



$$R_a = k_{m,n,p,q} [A]^m [B]^n [C]^p [D]^q - k_{r,s,t,v} [A]^r [B]^s [C]^t [D]^v \quad (20)$$

Versteeg et al. (1989) used Higbie's penetration model to describe the system in the liquid phase. Material balances for each species yielded four nonlinear partial differential

equations (PDEs). The concentration profiles are time dependent and were developed as a system of coupled nonlinear PDEs. These PDEs were subject to specified initial and two-point boundary conditions.

The model of Versteeg et al. (1989) satisfactorily explained the experimentally obtained absorption rates of CO_2 and H_2S in aqueous solutions of alkanolamines. Bosch et al. (1989) successfully applied the same model to interpret literature data for the absorption of CO_2 in sterically hindered amine solutions. However, the approximations made are of restricted use and can be applied to only a limited number of reactions. Furthermore, erroneous results occur when the linearization technique used is applied to reversible reactions.

Some mathematical models that describe simultaneous absorption of CO_2 and H_2S in an alkanolamine solution are presented in the literature (Haimour and Sandall, 1983; Bosch et al., 1989). The models of Haimour and Sandall (1983) describe the absorption of H_2S and CO_2 in secondary and tertiary amine solutions, in which interacting liquid phase reactions were taken into account. Haimour and Sandall (1983) assumed irreversibility and specific reaction rate expressions for the reactions involved, which suggests that these models are of limited use.

The penetration theory model presented by Bosch et al. (1989) describes simultaneous absorption of H_2S and CO_2 in mixtures of alkanolamines. Bosch et al.(1989) assumed reversibility, generalized reaction rate expressions, and generalized stoichiometry. Therefore, the general applicability of their model is limited only by the type of reactions modeled. However, some parallel and consecutive reactions were not taken into account in this model. Ionic species were involved in all reactions which take

place in aqueous amine solutions, but this model did not account for the concentration changes of these species.

Most models presented in the literature have not accounted for the coupling of the diffusion of ionic species. Diffusion of ionic species has been modeled similar to that of neutral species and electroneutrality maintained by applying a mean ion diffusivity. However, Littel et al. (1991) developed a numerical model based on Higbie's penetration theory to study the effect of the coupled diffusion of ions and parallel and consecutive reactions on the simultaneous absorption of H₂S and CO₂ in aqueous solutions of alkanolamines. The following reactions describe the system:



Littel et al. (1991) believed that the mass transfer rates of ionic species is greatly affected by the reverse reaction rates. Littel et al. (1991) also held that ionic species do not diffuse independently of each other, rather that the diffusion of ions is coupled to maintain electroneutrality throughout the system. The Nernst-Planck equation describes this coupling of the diffusion of ionic species.

Littel et al. (1991) compared their model with two of their less rigorous models. One of these less rigorous models described the diffusion of ionic species by assuming equal diffusivities for all ionic species, with the same reaction scheme used in the complex model. The second less rigorous model also assumed equal diffusivities, but took into account only the following direct reactions of CO₂ and H₂S.



Comparing these models they concluded that incorporating all relevant reactions in the mass transfer model instead of only the direct reactions between CO₂ and H₂S results only minor changes absorption rate predictions. However, incorporating the coupling of the diffusion of ions in the mass transfer model can result in a significant effect on the mass transfer rate of up to 20% (Littel et al., 1991). The model was solved numerically via the discretization technique described by Cornillesse et al. (1980) and is subject to the same large truncation errors.

The following is a summary of the literature survey:

- Mass transfer models that incorporate the coupling of the diffusion of ionic species can have a significant effect on the mass transfer rates.
- Incorporating all relevant reactions in the mass transfer model instead of taking a simplified view may not be practical.
- The choice of numerical methods may have a significant affect on the results.

For example, the large truncation errors which result from the method

described by Cornelisse et al. (1980) are introduced into the solution. If this truncation error is larger than the accepted error in the calculation, it would not be wise to use this numerical method. Therefore, careful choice of a numerical method is essential in obtaining credible concentration profiles.

Chapter 3

Diffusion Layer Modeling

3.1 Existing Diffusion Layer Model in DREAM

To model the mass transfer in downhole systems, expressions were developed to account for the flux of corrosive species through an annular film. The current mass transfer model in DREAM considers molecular diffusion and ion migration as the dominant mechanisms of mass transfer in the diffusion layer and incorporates both the concentration and electrical potential gradients in its formulation. A mass balance for a species in the diffusion layer can be written as (Sundaram et al., 1996):

$$D_{\text{eff}} \frac{d^2 c_i}{dy^{*2}} + z_i u_i F \frac{d}{dy^*} \left(c_i \frac{d\Phi}{dy^*} \right) = 0 \quad (33)$$

where

$$u_i = \frac{D_i}{RT} \quad (34)$$

There are two types of boundary conditions for Equation 33 at $y^* = \delta$: (1) the active wall, at which no corrosion product has formed; and (2) the non-active wall, in which a corrosion product has formed on the wall. For each of the two types of boundary conditions, there are two possibilities that can occur: (i) the species reacts at the wall and (ii) the species is nonreactive.

The second boundary condition at the turbulent layer-diffusion layer interface is given as (Sundaram et al., 1996):

$$c_i = c_{igd} \quad \text{at } y^* = 0. \quad (35)$$

If no corrosion product is formed (Newman, 1991),

$$D_{\text{mol}} \frac{dc_i}{dy^*} + z_i u_i F c_i \frac{d\Phi}{dy^*} = 0 \quad (36)$$

for nonreactive species, and

$$D_{\text{mol}} \frac{dc_i}{dy^*} + z_i u_i F c_i \frac{d\Phi}{dy^*} = \frac{i_i}{nF} \quad (37)$$

for reactive species (Sundaram et al., 1996; Newman, 1991).

Equation 33 with boundary condition 35 and either 36 or 37 is a system of nonlinear equations for which no analytical solution is known (Sundaram et al., 1996)

The system of equations which constitute the corrosion model are readily solved with the exception of the set of nonlinear differential equations resulting from the diffusion layer model. The electrical potential term in Equation 33 is an implicit function of concentration and can be eliminated by using the zero net current flow condition (Newman, 1991). The flux of any species through the diffusion layer can be expressed as (Sundaram et al., 1996):

$$J_j = -D_j \frac{dc_j}{dy^*} - z_j u_j F c_j \frac{d\Phi}{dy^*} \quad (38)$$

Applying the net current condition yields

$$\sum_j z_j J_j = 0 = -\sum_j D_j z_j \frac{dc_j}{dy^*} - \sum_j z_j^2 u_j F c_j \frac{d\Phi}{dy^*} \quad (39)$$

Rearranging Equation 39 gives

$$\frac{d\Phi}{dy^*} = -\frac{RT}{F} \frac{\sum_j z_j D_j \frac{dc_j}{dy^*}}{\sum_j D_j z_j^2 c_j} \quad (40)$$

Substituting Equation 40 into Equation 38 yields

$$\frac{d^2 c_i}{dy^{*2}} - z_i \frac{d}{dy^*} \left(c_i \frac{\sum_j z_j D_j \frac{dc_j}{dy^*}}{\sum_j z_j^2 D_j c_j} \right) = 0 \quad (41)$$

Introducing dimensionless length variables,

$$X = \frac{y^*}{\delta_D} \quad (42)$$

and taking the derivative of the bracketed term with respect to y^* results in (Sundaram et al., 1996):

$$\frac{d^2 c}{dX^2} + Sc = 0 \quad (43)$$

where

$$Sc = \frac{\left(\sum_{q=1}^{NC} z_q^2 D_q c_q \right) \left(\sum_{q=1}^{NC} z_q D_q \frac{d^2 c_i}{dX^2} \right) - \left(\sum_{q=1}^{NC} z_q^2 D_q \frac{dc_q}{dX} \right) \left(\sum_{q=1}^{NC} z_q D_q \frac{dc_q}{dX} \right)}{\left(\sum_{q=1}^{NC} z_q^2 D_q c_q \right)^2} \quad (44)$$

$$+ \frac{dc_i}{dX} \left(\frac{\sum_{q=1}^{NC} z_q D_q \frac{dc_q}{dX}}{\sum_{q=1}^{NC} z_q^2 D_q c_q} \right)$$

This model has been solved by a discretization technique using a second order finite-difference method (Liu, 1991; Cornelisse et al., 1980; Versteeg et al., 1989).

Although the existing model takes both concentration and potential gradients into account, the existing model and software has three problems. First, as stated previously, there are large roundoff errors associated with the discretization of this equation.

Therefore, another numerical method was sought.

Second, the corrosion rate (mils per year) is calculated by the following equation (DREAM 3.1)

$$\left[\frac{D_{\text{Fe}^{2+}} (c_{\text{Fe}^{2+}} - c_{\text{oFe}^{2+}})}{\delta} + \frac{c_{\text{Fe}^{2+}} (2FD_{\text{Fe}^{2+}})}{RT \left(\frac{d\Phi}{dx} \right)_{\text{avg}}} \right] \times 8.89 \times 10^8 \quad (45)$$

where 8.89×10^8 is a conversion factor from $\text{mol m}^{-2} \text{s}^{-1}$ to mils per year.

The first term of Equation 45 is always calculated incorrectly to be zero, since the concentration gradient in DREAM is always calculated as zero. The concentration gradient in the diffusion layer is zero as a result of the following:

- The concentration at each point in the diffusion layer is not calculated, rather, the value of the concentration at the turbulent layer-diffusion layer boundary is incorrectly assigned to the remaining points in the diffusion layer. Hence, there is no concentration gradient in the diffusion layer and the first term on the right hand side of Equation 45 is always erroneously zero.
- Secondly, the reaction flux at the wall of the reactive species is given by the following equations (Sundaram et al., 1996) based on the experimental data of de Waard and Milliams (1975) :

$$J_{r,CO_2} = -52.5 \exp\left(\frac{-5385}{T}\right) p_{CO_2} \quad (46)$$

$$J_{r,H_2S} = -9.8 \times 10^6 \exp\left(\frac{-9261}{T}\right) p_{H_2S} \quad (47)$$

Since the concentration does not change at each point in the diffusion layer, as previously mentioned, Equations 46 and 47 erroneously return only one value throughout the diffusion layer.

The second term on the right hand side of Equation 45 does not significantly contribute to the corrosion rate and, therefore, the corrosion rate remains zero. Last, the software does not return a value of zero for the corrosion rate because the labels “Corrosion Without Film” and “Corrosion With Film” were switched.

Therefore, a new approach to modeling mass transfer in the diffusion layer was initiated.

3.2 Proposed Diffusion Layer Model Development

The development of the diffusion layer mass transfer model follows Newman's (1991) development of the basic equations for the analysis of electrochemical systems. The flux, N_i , represents the number of moles passing per unit of time through a unit area oriented perpendicular to the velocity. In dilute solutions, the velocity of migration of an ion can be generalized to express the flux density of an ionic species as

$$N_i = c_i v_i = -z_i u_i F c_i \nabla \Phi - D_i \nabla c_i + c_i v \quad (48)$$

where,

$$u_i = \frac{D_i}{RT} \quad (49)$$

The first term on the right-most side of Equation 48 represents transport by migration. The second term represents transport by diffusion and is proportional to the gradient of concentration. The third term represents transport by convection. Since the diffusion layer is considered to be stagnant, migration and diffusion become the dominant modes of transport (Newman, 1991).

Using a species continuity equation, and taking into account the effect of the electrostatic potential gradient on the diffusion of ionic species, the following differential equation was developed by Littel et al. (1991) for each component i :

$$\frac{\partial c_i(y,t)}{\partial t} = D_i \frac{\partial^2 c_i(y,t)}{\partial y^2} - z_i D_i \frac{RT}{F} \frac{\partial(\Phi(y,t)c_i(y,t))}{\partial y} \quad (50)$$

Under the assumption of steady state, Equation 51 becomes

$$D_i \frac{d^2 c_i}{dy^2} = z_i D_i \frac{RT}{F} \frac{d(\Phi c_i)}{dy} \quad (51)$$

where Φ represents the electrostatic potential gradient which couples the diffusion of ionic species. The potential can be expressed as a function of ion concentrations and diffusivities (Newman, 1991; Littel et al., 1991) as follows:

$$\Phi(y) = \frac{F}{RT} \frac{\sum_{q=1}^{NC} z_q D_q \frac{\partial c_q}{\partial y}}{\sum_{q=1}^{NC} z_q^2 D_q C_q} \quad (52)$$

Substitution of Equation 52 into Equation 51 gives

$$D_i \frac{d^2 c_i}{dy^2} = -z_i D_i \frac{d}{dy} \left[\frac{\sum_{q=1}^{NC} z_q D_q \frac{dc_q}{dy}}{\sum_{q=1}^{NC} z_q^2 D_q c_q} C_i \right] \quad (53)$$

Expanding the first term on the right hand side of Equation 53 and introducing dimensionless length variables from Equation 42, results in

$$D_i \frac{d^2 c_i}{dX^2} = z_i D_i \left[\frac{\left(\sum_{q=1}^{NC} z_q^2 D_q c_q \right) \left(\sum_{q=1}^{NC} z_q D_q \frac{d^2 c_q}{dX^2} \right) - \left(\sum_{q=1}^{NC} z_q^2 D_q \frac{dc_q}{dX} \right) \left(\sum_{q=1}^{NC} z_q D_q \frac{dc_q}{dX} \right)}{\left(\sum_{q=1}^{NC} z_q^2 D_q c_q \right)^2} + \frac{dc_i}{dX} \left(\frac{\sum_{q=1}^{NC} z_q D_q \frac{dc_q}{dX}}{\sum_{q=1}^{NC} z_q^2 D_q c_q} \right) \right] \quad (54)$$

To this point, the derivation of Equation 54 is similar to that of the existing model in DREAM (see Equation 44) except for the reaction term. To simplify Equation 54, let

$$y_{i1} = c_i, \quad y_{i2} = \frac{dc_i}{dX} \quad (55)$$

$$\sigma_1 = \sum_{j=1}^{NC} z_j D_j y_{j2} \quad (56)$$

$$\sigma_2 = \sum_{j=1}^{NC} z_j^2 D_j y_{j1} \quad (57)$$

$$\sigma_3 = \sum_{j=1}^{NC} z_j^2 D_j y_{j2} \quad (58)$$

Substituting Equations 55-58 into Equation 54 gives

$$\frac{dy_{j2}}{dX} - z_j y_{j2} \frac{\sigma_1}{\sigma_2} - z_j y_{j1} \left[\frac{\left(\sum_{j=1}^{NC} z_j D_j \frac{dy_{j2}}{dX} \right) \sigma_2 - \sigma_1 \sigma_3}{\sigma_2^2} \right] = 0. \quad (59)$$

Further expansion gives

$$\frac{dy_{i2}}{dX} - \frac{z_i y_{i1}}{\sigma_2} \sum_{j=1}^{NC} z_j D_j \frac{dy_{j2}}{dX} - z_i y_{i2} \frac{\sigma_1}{\sigma_2} + z_i y_{i1} \frac{\sigma_1 \sigma_3}{\sigma_2^2} = 0. \quad (60)$$

In order to eliminate the second derivative on the right-hand side of Equation 54, the summation in Equation 60 must be separated into

$$\sum_{j=1}^{NC} z_j D_j \frac{dy_{i2}}{dX} = z_i D_i \frac{dy_{i2}}{dX} + \sum_{j \neq i}^{NC} z_j D_j \frac{dy_{j2}}{dX} \quad (61)$$

Substituting Equation 61 into Equation 60 gives

$$\left[1 - \left(\frac{z_i y_{i1}}{\sigma_2} \right) (z_i D_i) \right] \frac{dy_{i2}}{dX} - \frac{z_i y_{i1}}{\sigma_2} \sum_{j \neq i}^{NC} z_j D_j \frac{dy_{j2}}{dX} - z_i y_{i2} \frac{\sigma_1}{\sigma_2} + z_i y_{i1} \frac{\sigma_1 \sigma_3}{\sigma_2^2} = 0 \quad (62)$$

The first set of boundary conditions for each component i at the turbulent layer-diffusion layer is given as follows:

$$c_i(x) = c_{i,bulk} \quad \text{at } X = 0 \quad (63)$$

The second set of boundary conditions is classified into two categories: (i) those for nonreactive species, and (ii) those for reactive species and is given by the following equation (Newman, 1991, Littel et al., 1991).

At $X = \delta$;

$$D_j \left(\Phi(X) c_j(X) \right) + \frac{z_i D_i F}{RT} \frac{d\Phi}{dX} c_i = \begin{cases} 0 & \text{For nonreactive species} \\ \delta R_i & \text{For reactive species} \end{cases} \quad (64)$$

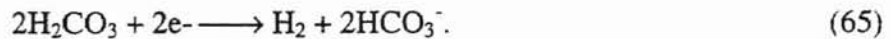
The species charge, z_i , and temperature, T , are constants. The values for D_i were obtained from the turbulent layer calculations (DREAM v.3.1). The bulk concentrations used for the first set of boundary conditions were found from the turbulent-diffusion layer boundary.

Equation 62 was solved numerically as a two-point boundary value problem through a shooting method using a fifth order Runge-Kutta method with a truncation error of Δh^5 , and a Newton-Raphson convergence method (Press et al., 1997). The flux calculated in the turbulent layer model was used as an “estimate” for the first iteration.

3.3 Determination of the Boundary Conditions for Reactive Species

The boundary condition, R_i in Equation 64, is nonzero for the reactive species, Fe^{2+} , HCO_3^- , and HS^- . There are two methods of calculating the flux at the wall for the reactive species.

Method I. The following reactions are assumed to occur on the metal surface for this model (de Waard and Milliams, 1975, Morris et al., 1980, Liu, 1991, Sundaram et al., 1996), the:



A similar reaction can be written for H_2S :



Sundaram et al. (1991) modified the de Waard and Milliams (1975) flux equation for CO_2 and included a CO_2 partial pressure correction:

$$J_{\text{CO}_2} = J_{\text{HCO}_3^-} = -52.5 \exp\left(\frac{-5385}{T}\right) P_{\text{CO}_2} \quad (67)$$

Similarly for H_2S (Sundaram et al., 1991),

$$J_{\text{H}_2\text{S}} = J_{\text{HS}^-} = -9.8 \times 10^6 \exp\left(\frac{-9261}{T}\right) P_{\text{H}_2\text{S}} \quad (68)$$

The Fe^{2+} flux can be found from the contributions from both the CO_2 and H_2S in the system (Sundaram et al., 1996).

$$J_{\text{Fe}^{2+}} = 2(J_{\text{CO}_2} + J_{\text{H}_2\text{S}}) \quad (69)$$

If there is no H₂S present, only CO₂ contributes.

Although this method is sensitive to temperature, only temperature and partial pressures of CO₂ and/or H₂S are used; no pH corrections were made to this equation. Therefore, it is insensitive to both the pH and errors in the water analysis. The errors in the water analysis will, however, be reflected in the bulk properties via Equation 50.

Method II. The reaction term at the wall, R_i, can also be found from the reaction current density (Liu, 1991; Bockris and Reddy, 1970; Newman, 1991). The Butler-Volmer expression (Bockris and Reddy, 1970; Newman, 1991) can be applied to kinetics of system reactions. For the anodic reaction, (Fe → Fe²⁺ + 2e⁻),

$$i_a = i_{a0} \exp(\alpha_a F \eta_a / RT) \quad (70)$$

where $\eta_a = E_{\text{corr}} - E_a$, and for the cathodic reaction, (2H⁺ + 2e⁻ → H₂),

$$i_c = i_{c0} \exp(\alpha_c F \eta_c / RT) \quad (71)$$

where $\eta_c = E_{\text{corr}} - E_c$.

For the anodic reaction, the equilibrium potential can be derived from the Fe²⁺/Fe electrode reaction which has an equilibrium potential (Bockris and Reddy., 1970)

$$E_a = -0.44 + \frac{RT}{2F} \ln[\text{Fe}^{2+}]. \quad (72)$$

The equilibrium potential at the cathode can be calculated as (Bockris and Reddy, 1970):

$$E_c = 0 + \frac{RT}{2F} \ln[\text{H}^+]. \quad (73)$$

The rate of corrosion of a metal is given directly by the rate of metal dissolution. Therefore, the corrosion current is equal to the metal-dissolution current.

$$I_{\text{corr}} = I_a \quad (74)$$

If it is assumed that the cathodic and anodic reactions have equal surface areas over which these reactions occur, the following relation is true (Bockris and Reddy, 1970).

$$i_{\text{corr}} = i_a = -i_c \quad (75)$$

This assumption is applicable to a metal corroding by a Wagner-Traud mechanism (Bockris and Reddy, 1970). The essence of the Wagner-Traud mechanism is that, for corrosion to occur, the electron-sink and electron-source areas on the corroding metal do not have to be spatially separated. Therefore, impurities or other surface imperfections can be present, but are not required for corrosion to occur. The necessary and sufficient condition for corrosion is that the metal dissolution reaction and some electronation reaction proceed simultaneously at the metal-environment interface (Bockris and Reddy, 1970).

By knowing E_a and E_c and the other parameters in Equations 57-60, E_{corr} can be calculated by substituting Equations 70-73 into Equation 75 thereby giving i_a and i_c , the reaction current densities:

$$i_{\text{ao}} \exp\left(\frac{\alpha_a F(E_{\text{corr}} - E_a)}{RT}\right) = i_{\text{co}} \exp\left(\frac{\alpha_c F(E_{\text{corr}} - E_c)}{RT}\right) \quad (76)$$

$$(\ln i_{\text{ao}}) \frac{\alpha_a F(E_{\text{corr}} - E_a)}{RT} = (\ln i_{\text{co}}) \frac{\alpha_c F(E_{\text{corr}} - E_c)}{RT} \quad (77)$$

$$(\ln i_{\text{ao}})(E_{\text{corr}} - E_a) = (\ln i_{\text{co}})(E_{\text{corr}} - E_c) \quad (78)$$

$$E_{\text{corr}} - E_a = \frac{\ln(i_{\text{co}})\alpha_c}{\ln(i_{\text{ao}})\alpha_a} (E_{\text{corr}} - E_c) \quad (79)$$

$$E_{corr} = E_a + \frac{\ln(i_{co})\alpha_c}{\ln(i_{ao})\alpha_a} (E_{corr} - E_c) \quad (80)$$

$$E_{corr} - \frac{(\ln i_{co})\alpha_c}{(\ln i_{ao})\alpha_a} (E_{corr} - E_c) = E_a \quad (81)$$

$$E_{corr} - \frac{\ln(i_{co})\alpha_c}{\ln(i_{ao})\alpha_a} E_{corr} + \frac{\ln(i_{co})\alpha_c}{\ln(i_{ao})\alpha_a} E_c = E_a \quad (82)$$

$$E_{corr} \left[1 - \frac{\ln(i_{co})\alpha_c}{\ln(i_{ao})\alpha_a} \right] = E_a - \frac{\ln(i_{co})\alpha_c}{\ln(i_{ao})\alpha_a} E_c \quad (83)$$

$$E_{corr} = \frac{E_a - \frac{\ln(i_{co})\alpha_c}{\ln(i_{ao})\alpha_a} E_c}{\left[1 - \frac{\ln(i_{co})\alpha_c}{\ln(i_{ao})\alpha_a} \right]} \quad (84)$$

Values for i_{ao} ($2.00 \times 10^{-7} \text{ mA/cm}^2$) and i_{co} ($4.00 \times 10^{-6} \text{ mA/cm}^2$) were obtained from Gray et al. (1989) and Morris et al. (1980), respectively. Values for α_a and α_b were obtained from Newman (1991). The reaction current density is directly proportional to the to the reaction flux and units can be easily converted from A/cm^2 to $\text{moles/m}^2 \cdot \text{s}$ as follows (Newman, 1991; Bockris and Reddy, 1970):

$$\frac{i}{nF} = \frac{\text{mA}}{\text{cm}^2} \times \frac{1}{96500} \frac{\text{mole}}{\text{A} \cdot \text{s}} \times \left(\frac{100\text{cm}}{\text{m}} \right)^2 \times \frac{\text{A}}{1000\text{mA}} = \frac{\text{mol}}{\text{m}^2 \cdot \text{s}} \quad (85)$$

3.4 Comparison of Boundary Conditions

Concentration profiles for Fe^{2+} and HCO_3^- resulting from each method of determining boundary conditions were obtained for three temperatures: 150°F, 200°F, and 300°F, which represent the wellhead, middle and bottomhole temperatures, respectively.

The concentration profiles for Method I were then compared to those of Method II.

Figures 2-5 illustrate the results.

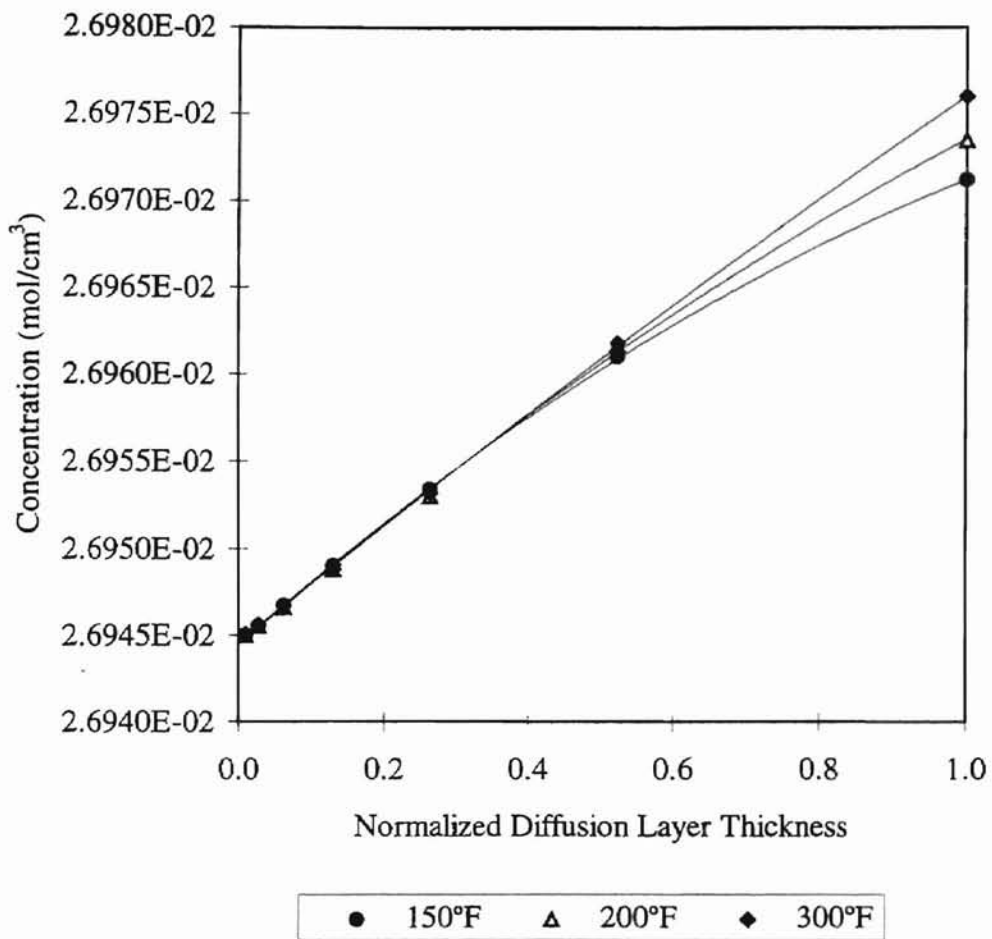


Figure 2. Fe⁺⁺ Concentration vs. Normalized Diffusion Layer Thickness for the de Waard and Milliams Method

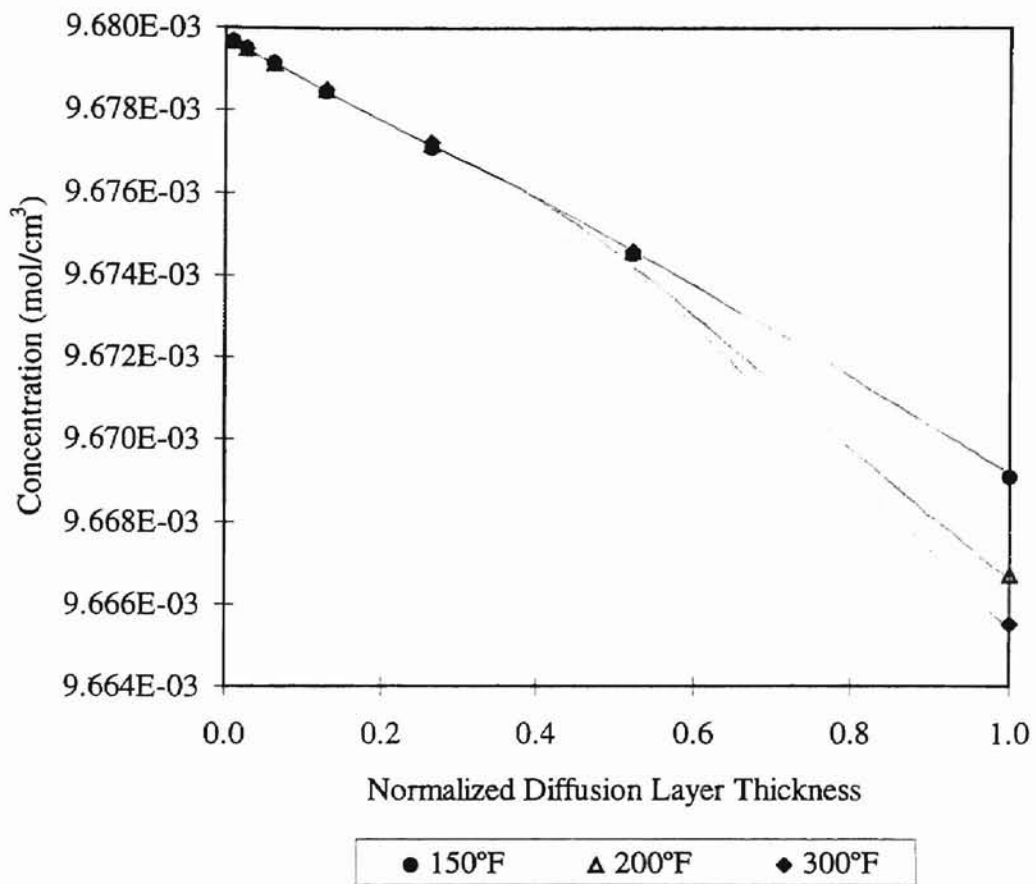


Figure 3. HCO₃⁻ Concentration vs. Normalized Diffusion Layer Thickness for the de Waard and Milliams Method

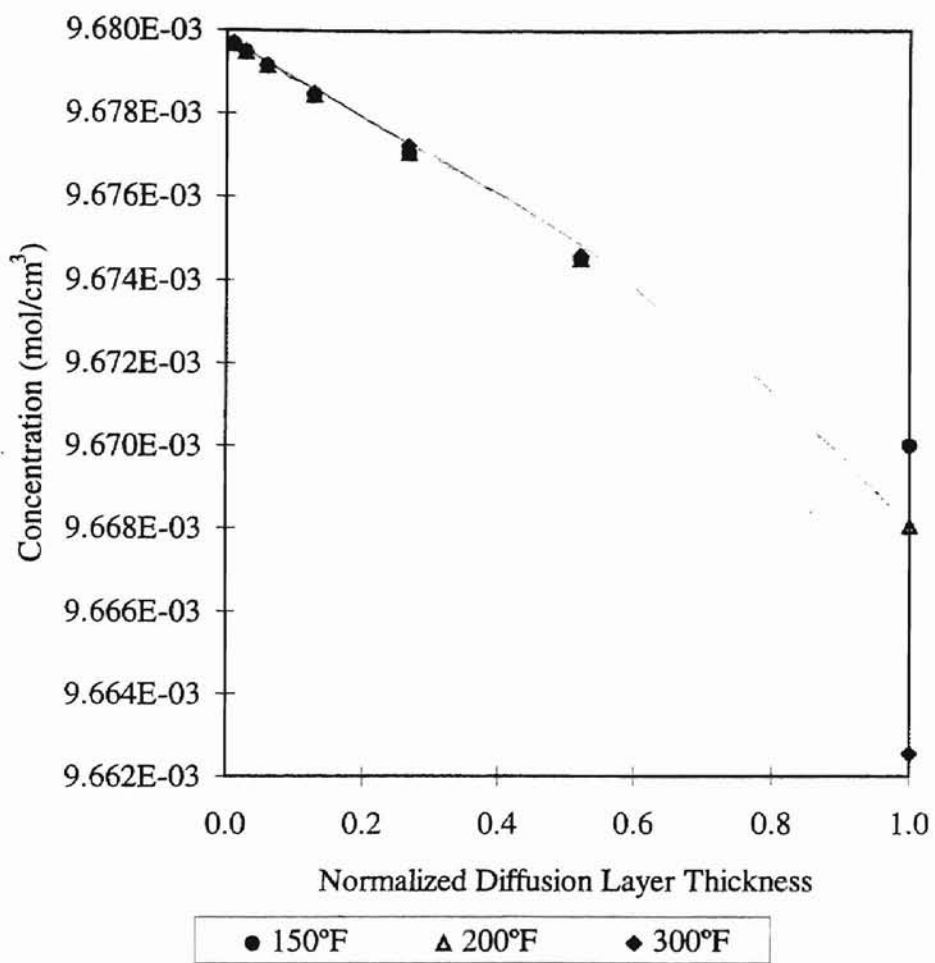


Figure 5. HCO_3^- Concentration vs. Normalized Diffusion Layer Thickness for the Current Density Method

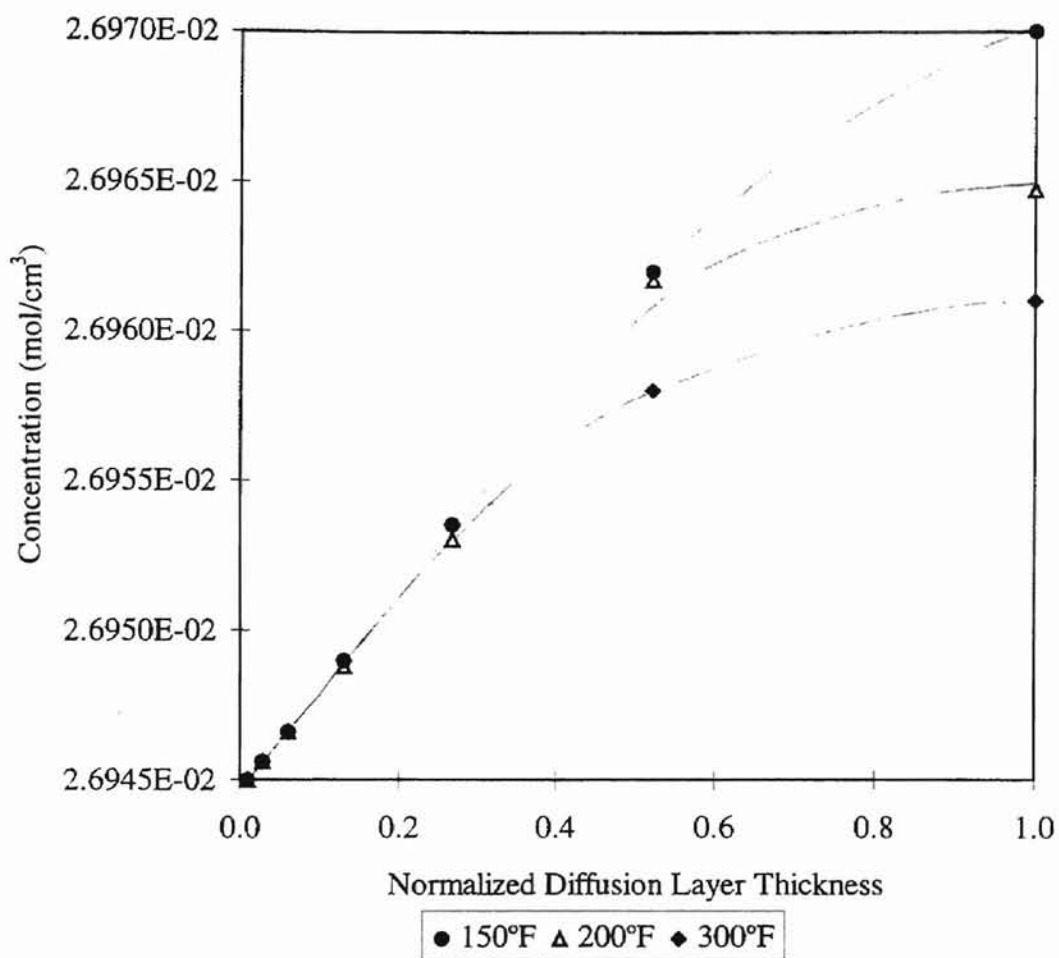


Figure 4. Fe⁺⁺ Concentration vs. Normalized Diffusion Layer Thickness for the Current Density Method

In Figures 2, and 4, the concentration of ferrous ion increases while moving toward the wall. The concentration profiles from Method I (Figure 2) and Method II (Figure 4), exhibit a change in the concentration profile with respect to temperature. The concentration of iron is identical for the first two-thirds of the diffusion layer for the first two temperatures evaluated. However, the resulting concentration of iron at the wall varies with respect to temperature: the highest concentration of iron corresponds to the lowest temperature evaluated. Figures 2 and 4 show that the concentration of ferrous ion decreases when moving down a well. Therefore, the concentration of ferrous ion decreases with increasing temperature.

In Figures 3 and 5, the concentration of bicarbonate decreases while moving toward the wall. The concentration profile for Method I (Figure 3) shows only a slight change in concentration of HCO_3^- with respect to temperature. The concentration profiles for Method II, (Figure 5), show a slightly greater change in the concentration of HCO_3^- with respect to temperature than for Method I. However, both Method I and Method II returned virtually the same concentration profiles for HCO_3^- .

In summary, Method II for determining boundary conditions results in more realistic concentration profiles in the diffusion layer for the ferrous ion. As mentioned before, Method II yields a lower concentration of ferrous ion for higher temperature, whereas Method I does not. Therefore, the complete diffusion layer model includes Method II; evaluation of the boundary conditions via current density calculations. This method was also chosen because it relies on fundamental principles in its derivation, whereas, Method I is an empirical formulation used to fit laboratory data.

Chapter 4

Results

4.1 Comparison of Corrosion Rates

The proposed diffusion layer model, with boundary conditions calculated via Method II, was used to calculate the corrosion rate for three actual wells from the same field using data from caliper surveys obtained through regular well maintenance. These caliper surveys showed no clear trends in corrosivities, rather scattered pitting concentrating on the upper portion of the wells. The cases studied are for gas wells that had been in production for a period of time and had never been treated with inhibitors (Sundaram et al. 1996). In all the cases, low carbon steel was used as the tubing material. It should be noted that this model development is based on the assumption of uniform corrosion which rarely occurs. Therefore, in this sense a direct comparison cannot be made. However, the model should give a practical guide to the prediction of corrosion rates.

Case 1. The upper portion of the well in Case 1 is considered corrosive. In particular, the concentrations of carbon dioxide and dissolved solids are high. These high concentrations of corrosive species combined with significant water production provides an environment conducive to corrosion. Field data indicate that corrosion was observed to begin around 1800 m. Below 1800 m, the caliper survey reported corrosion rates below the detection threshold of 200 $\mu\text{m}/\text{yr}$. Table 1 gives the gas well conditions for this case.

Table 1
Well Specifications for Case 1

Well Conditions		Constituent	ppm	Component	Mole %
Water Production	28 B/D	Sodium	6490	Methane	90.94
Gas Production	2150 MSCFD	Calcium	298	Ethane	4.37
Wellhead		Magnesium	38	Propane	1.14
Temperature	130 °F	Barium	4	Isobutane	0.27
Pressure	1890 psia	Strontium	0	n-butane	0.23
Bottomhole		Potassium	0	Isopentane	0.13
Temperature	290 °F	Iron	36	n-pentane	0.08
Pressure	4000 psia	Chloride	10100	Hexane	0.11
		Sulfate	111	Hexanes +	0.27
Depth	9700 ft.	Carbonate	0	Nitrogen	0.25
Tubing ID	2.441 in.	Bicarbonate	879	Carbon Dioxide	2.21

Case 2. The well in Case 2 has a relatively high carbon dioxide concentration of 1.26%. The caliper survey data indicates a moderate corrosion rate in the upper portions of the well. The gas well conditions for this case are summarized in Table 2.

Case 3. Case 3 was chosen to test the accuracy of the model in a noncorrosive well. As has been pointed out by Crolet (1993), the accurate prediction of corrosion includes not only predicting when corrosion will occur, but also predicting the lack of it. The caliper data showed corrosion rates below the detection threshold of the caliper device (200 $\mu\text{m}/\text{yr}$). Table 3 gives the gas well conditions for this case.

The flux at the wall for these cases was calculated via Equation 85 and converted to mm/yr by the following equation

$$\frac{\text{mol}}{\text{cm}^2 \cdot \text{s}} \times \frac{31536000\text{s}}{\text{yr}} \times \frac{\text{cm}^3}{7.8\text{g}} \times \frac{55.847\text{g}}{\text{mol}} \times \frac{10\text{mm}}{1\text{cm}} = \frac{\text{mm}}{\text{yr}} \quad (86)$$

The results of the proposed model were then compared with (i) an empirical model (de Waard and Milliams 1975), (ii) the values currently calculated from DREAM using the existing diffusion layer model, (iii) and the field data. The results of this comparison are presented in Table 4.

Table 4 compares the corrosion rates of each case at three different temperatures, which represents the top, middle, and bottom of a well. The corrosion rates were calculated using the previously discussed methods. The field data, as mentioned before, do not show clear trends in corrosivity. Therefore, Table 4 gives a range encompassing the variation in the field data.

All model predictions in Table 4 calculate the corrosion rate in the absence of a corrosion product layer. Considering the complex phenomena for the downhole corrosion

Table 2
Well Specifications for Case 2

Well Conditions		Constituent	ppm	Component	Mole %
Water Production	27 B/D	Sodium	6280	Methane	91.6
Gas Production	1352 MSCFD	Calcium	454	Ethane	4.39
Wellhead		Magnesium	50	Propane	1.18
Temperature	130 °F	Barium	2	Isobutane	0.33
Pressure	1440 psia	Strontium	0	n-butane	0.25
Bottomhole		Potassium	0	Isopentane	0.14
Temperature	290 °F	Iron	0	n-pentane	0.09
Pressure	4000 psia	Chloride	10300	Hexane	0.13
		Sulfate	196	Hexanes +	0.33
Depth	9450 ft.	Carbonate	0	Nitrogen	0.3
Tubing ID	2.441 in.	Bicarbonate	313	Carbon Dioxide	1.26

Table 3
Well Specifications for Case 3

Well Conditions		Constituent	ppm	Component	Mole %
Water Production	124 B/D	Sodium	127	Methane	90.1
Gas Production	2800 MSCFD	Calcium	21	Ethane	6
Wellhead		Magnesium	0	Propane	1.68
Temperature	130 °F	Barium	2	Isobutane	0.45
Pressure	1440 psia	Strontium	0	n-butane	0.34
Bottomhole		Potassium	0	Isopentane	0.2
Temperature	290 °F	Iron	0	n-pentane	0.18
Pressure	4000 psia	Chloride	195	Hexane	0.4
		Sulfate	0	Hexanes +	0.22
Depth	9700 ft.	Carbonate	0	Nitrogen	0.31
Tubing ID	2.88 in.	Bicarbonate	60	Carbon Dioxide	0

process the proposed model gives good estimates for the corrosion of wells in various environments. All three models show an increase in the corrosion rate when moving down a well. Although this is incorrect from field experience, the values obtained still provide a prediction of how corrosive a well will be. The magnitudes of the corrosion rates obtained using the de Waard and Milliams (1975) model are not realistic. For example, this model reports that the well in Case 1 would have a maximum corrosion rate of 1100 mm/yr.

The model used in DREAM predicted extremely high corrosion rates for all three cases considered. Since this model is the modified de Waard and Milliams (1975) model with a partial pressure modification (Sundaram et al., 1996), it is susceptible to the same dependency on CO₂ partial pressure. The model used in DREAM also predicts that the well in Case 1 is more corrosive than the well in Case 2 which is more corrosive than the well in Case 3. However, it does not predict when very little corrosion will occur.

For wells with annular flow, the proposed model gives good correlation with the field data. The corrosion rate predictions for the most corrosive well, Case 1, are slightly lower than the maximum observed corrosion rate from the caliper survey. However, the predicted corrosion rates are well within the range of corrosivities encompassing the field data. The proposed model shows a significant decrease in the predicted corrosion rate for Case 3 compared to the values returned by DREAM or the De Waard and Milliams (1975) model. Therefore, the proposed model not only predicts when a high corrosion rate is probable, but also when a low corrosion rate will occur. The ability to give good correlation to field data for high, medium, and low corrosivities is a significant improvement over the existing model in DREAM. Although the general approach to

modeling was not changed, two differences exist in the model used in DREAM and the proposed model. The addition of a reaction term in the species continuity equation allowed for the reacting species at the wall to be considered. Employing the current density calculations as boundary conditions resulted in corrosion rates closer to the range observed in the field data than the values currently calculated in DREAM. These changes produced a model that predicts the corrosion rates very close to the actual field data.

Table 4					
Comparison of Corrosion Rate Predictions					
Corrosion Rate (mm/yr)					
Case Number	Temperature (°F)	DREAM v. 3.1	de Waard & Milliams (1975)	Proposed Model	Field Data
1	150	5.7	7.9	0.9	0.2-3.6
	200	32	1.9	1.3	
	290	1100	130	3.2	
2	150	2.4	4.9	0.4	0.1-0.80
	200	17	20	1.1	
	290	42	43	2.1	
3	150	0.7	1.7	0.4	<0.2
	200	4.7	11	0.7	
	290	13	33	1.3	

Chapter 5

Conclusions and Recommendations

5.1 Conclusions

The following conclusions were drawn at the end of this research:

- A mathematical model for modeling the diffusion layer in downhole natural gas systems has been developed. This model relies on fundamental principles in its formulation and takes into account the reaction of active species at the wall in the boundary conditions.
- The numerical method used to solve this model relies on a fifth order Runge-Kutta method and a Newton-Raphson convergence method (Press et al., 1997). This numerical method results in less round-off error than the second-order discretization technique presently used in DREAM.
- The proposed model greatly surpasses the de Waard and Milliams (1975) model in predicting corrosion rates for the downhole wells modelled.
 1. The de Waard and Milliams (1975) model uses bulk concentrations to calculate the corrosion rate, therefore, there is no need to model the diffusion layer. However, the proposed model takes into account the reaction mechanism at the surface and uses surface concentration to calculate the corrosion rate.
 2. The corrosion rates calculated from the proposed model also give good agreement with field data. Not only is corrosion predicted for

both medium to highly corrosive wells, but also when low corrosion occurs.

3. The de Waard and Milliams (1975) equation can only be applied to systems that have a CO₂ partial pressure less than 2 bars (de Waard and Milliams 1975, de Waard and Lotz 1993).
 4. The de Waard and Milliams (1975) equation assumes no mass transfer effects. This assumption is in error since an increase in both gas and liquid flow rates in a two-phase flow system will yield a substantial increase in the corrosion rate.
- As has been stated by Crolet (1993), the accurate prediction of corrosion includes not only predicting when corrosion will occur, but also predicting the absence of corrosion. The proposed model not only predicted corrosion for highly corrosive wells, but also gave good agreement with field data for downhole wells with low to moderate corrosion.

5.2 Recommendations

- It is recommended that the proposed model be implemented into DREAM.
- It is also recommended to model wells with widely varying conditions such as gas and water production rates and temperature to obtain the limitations of the model.
- The pH calculation in DREAM is for a non-buffered solution which makes the pH predictions quite low. Although this should be a point of reexamination, it does not affect the results of the proposed model as it is insensitive to the actual pH calculation.

- Localized corrosion, in practice, is more difficult to predict than uniform corrosion but it is also more important. Localized corrosion is also defined as the partial attack of a metal surface. Caliper surveys indicate that this partial surface attack appears in the zone of water vapor condensation and near pipe joints and fittings. Localized corrosion can also occur between pipe and corrosion product layers. If the periodic up and down liquid film flow causes fatigue in the corrosion product film, a localized attack can occur. Therefore, in order to fully model the corrosion in downhole natural gas wells, it would be practical to add a localized corrosion model.

References

- Al-Ghawas H.A. and Sandall O.C. (1988), Modeling the Simultaneous Transport of Two Acid Gases in Tertiary Amines with Reversible Reactions, *Sep. Sci. Techn.*, **23**, 1523-1540.
- Bacon T.S. and Brown E.A. (1943), Corrosion in Distillate Wells, *Oil & Gas J*, **41** No. 49, 91-92.
- Baker G.A. and Oliphant T.A. (1960) *Quant. Appl. Mth*, **17**(4),361.
- Bard A.J., and Faulkner L.R. (1985), Electrochemical Methods: Fundamentals and Applications, John Wiley, New York, 429-433.
- Bilhartz H.L. (1952), Sweet Oil Well Corrosion, *Pet. Eng.* Sept, B, 78-88.
- Bird, Stewart, and Lightfoot (1960), Transport Phenomena, John Wiley, New York..
- Bockris J.O.M. and Reddy A.K.N. (1970), Modern Electrochemistry, Plenum Press, New York, Vol. 1-2.
- Bosch H., Versteeg G.F. and Van Swaaij W.P.M. (1989), Gas-Liquid Mass Transfer with Parallel Reversible Reactions—I. Absorption of CO₂ Into Solutions of Sterically Hindered Amines, *Chem. Eng. Sci.*, **44**, 2735-2743.
- Bosch H., Versteeg G.F. and Van Swaaij W.P.M. (1989), Gas-Liquid Mass Transfer with Parallel Reversible Reactions—II. Absorption of CO₂ Into Amine-Promoted Carbonate Solutions, *Chem. Eng. Sci.*, **44**, 2745-2750.
- Cornelisse R., Beenackers A.C.M., Van Beckum F.P.H. and van Swaaij W.P.M. (1980), Numerical Calculation of Simultaneous Mass Transfer of Two Gases Accompanied by Complex Chemical Reactions, *Chem. Eng. Sci.*, **35**, 1245-1260.
- Crolet J.L (1993), *J. Mat. Sci.*, **28**, 2589-2606.
- Crolet J. L. (1993), Which CO₂ Corrosion? Hence Which Prediction?, 10th European Corrosion Congress, Barcelona 5-9 July 93, **1**, 473-497, London, UK, European Federation of Corrosion, 1993.
- Crolet J.L. 1983), *J. Petril. Techn.*, August, 1553-1558.
- Davies D.H. and Burstein G.T. (1980) *CORROSION* **36**, 416.

- De Waard C. and Lotz U. (1993), Prediction of CO₂ Corrosion of Carbon Steel, CORROSION/93, paper no. 640, Houston, TX, NACE.
- De Waard C. and Milliams D.E. (1975), Carbonic Acid Corrosion of Steel, *Corrosion*, **31**, 177-181.
- DREAM v3.1 FORTRAN Code
- Dugstad, A. (1992), The Importance of FeCO₃ Supersaturation on the CO₂ Corrosion of Carbon Steels, CORROSION/92, Paper no. 14, Houston, TX, NACE.
- Glasscock D.A. and Rochelle G.T. (1989), Numerical Simulation of Theories for Gas Absorption with Chemical Reaction, *A.I.Ch.E. J.*, **35**, 1271-1281.
- Gray L.G.S., Anderson B.G., Danysh M.J., and Tremaine P.R. (1989), Mechanisms of Carbon Steel Corrosion in Brines Containing Dissolved Carbon Dioxide at pH 4, Corrosion/89, Paper No. 464, New Orleans.
- Greco E.C. and Wright W.B. (1962), *Corrosion*, **18**, 119-124.
- Greenwell H.E. (1952), Studies of Water Dependent Corrosion of Steel, *Corrosion*, May, 177-181.
- Hackerman N. and Schmidt H.R. (1949), Kinetics of the Corrosion Process in Condensate Gas Wells, *Ind. & Eng. Chem.*, August, 1712-1716.
- Haimour N. and Sandall O.C. (1983), Selective Removal of Hydrogen Sulfide and Carbon Dioxide Using Diethanolamine, *Sep. Sci. Techn.*, **18**, 1221-1249.
- Kvarkevål J. (1997), A Kinetic Model for Calculating Concentration Profiles and Fluxes of CO₂-Related Species Across the Nernst Diffusion Layer, CORROSION/97, paper no. 5, Houston, TX, NACE.
- Little R.J., Filmer B., Versteeg G. F. and Van Swaaij W.P.M. (1991), Modeling of Simultaneous Absorption of H₂S and CO₂ in Alkanolamine Solutions: The Influence of Parallel and Consecutive Reversible Reactions and the Coupled Diffusion of Ionic Species, *Chem. Eng. Sci.*, **46**, 2303-2313.
- Liu G.H. (1991), A Mathematical Model For Prediction of Downhole Gas Well Uniform Corrosion in CO₂ and H₂S Containing Brines, Ph.D. Thesis, Oklahoma State University.
- Morris D.R., Sampaleanu L.P., and Veysey D.N. (1980), The Corrosion of Steel by Aqueous Solutions of Hydrogen Sulfide, *J. Electrochem. Soc.*, **127**, 1228-1235.

Nesic, S., Solvi G.T., Enerhaug J. (1995), Comparison of the Rotating Cylinder and Pipe Flow Tests for Flow-Sensitive Carbon Dioxide Corrosion, *Corrosion Science*, **51**, 773-787.

Newman, John S. (1991), Electrochemical Systems, 2nd ed., Prentice Hall, New Jersey.

Perry R.H., Green D.W., and Maloney J.O. (1984), Perry's Chemical Engineers' Handbook, 6th ed., McGraw-Hill, New York.

Press J. (1995) Numerical Recipes in FORTRAN, 2nd ed. Cambridge University Press, NY.

Schmitt G. and Rothman B. (1984), Studies on the Corrosion Mechanism of Unalloyed Steel in Oxygen-Free Carbon Dioxide Solutions, Part I. Kinetics of the Liberation of Hydrogen, *CO₂ Corrosion in Oil and Gas Production--Selected Papers, Abstracts and References*, NACE, 154-166.

Sundaram M., Raman V., High M.S., Tree D.A. and Wagner J. (1996), Deterministic Modeling of Corrosion in Downhole Environments, CORROSION/96, paper no. 30, Houston, TX, NACE.

Tewari P.H., and Campbell A.B. (1979), Dissolution of Iron During the Initial Corrosion of Carbon Steel in Aqueous H₂S Solutions, Can. J. Chem., **57**, 188-196.

Trethewey, Kenneth R. and Roberge, Pierre R. (1993), Modeling of Aqueous Corrosion, From Individual Pits to System Management, Kluwer Academic Publishers, Boston, 1-12.

Versteeg G.F., Kuipers J.A.M., Van Beckum F.P.H. and Van Swaaij W.P.M. (1989), Mass Transfer with Complex Reversible Chemical Reactions—I. Single Reversible Chemical Reaction, *Chem. Eng. Sci.*, **44**, 2295-2310.

Versteeg G.F., Kuipers J.A.M., Van Beckum F.P.H. and Van Swaaij W.P.M. (1989), Mass Transfer with Complex Reversible Chemical Reactions—II. Parallel Reversible Chemical Reaction, *Chem. Eng. Sci.*, **44**, 2295-2310.

Wieckowski A. and Ghali E. (1983), *Electrochemical Acta*, **28**, No. 11, 1619-1626.

Appendix

FORTRAN Code for the Mass Transfer Calculations in the Diffusion Layer

SAMPLE INPUT DATA

Species	Charge	Deff(dm ² /s)	Cio(mol/dm ³)	dco/dx
Na+	1	2.788605E-07	2.822805E-01	0
Ca++	2	1.655073E-07	7.435130E-03	0
Mg++	2	1.475011E-07	0.001563143	0
Ba++	2	1.770013E-07	2.913329E-05	0
Sr++	2	1.405434E-07	0	0
K+	1	4.091067E-07	0	0
Fe++	2	1.502841E-07	2.694464E-02	3.314041E-2
Cl-	-1	4.247473E-07	2.849083E-01	0
SO4--	-2	2.226431E-07	1.155528E-03	0
CO3--	-2	1.928646E-07	2.703652E-10	0
HCO3-	-1	2.476905E-07	9.679772E-03	1.005385E-2
H+	1	1.947014E-06	2.551950E-04	0
OH-	-1	1.099857E-06	5.051893E-10	0
HS-	-1	3.617950E-07	0	0
S--	-2	2.226431E-07	0	0
CO2	0	3.711008E-07	5.781635E-02	6.710422E-3
H2S	0	3.118133E-07	0	0

SAMPLE OUTPUT

The output prints out the interval for which the calculation is performed, x(i), and then prints out the concentration values, y(i)

```
.10099E-01
y(i)
.540695E-02
.523952E-03
.000000E+00
.145666E-04
.000000E+00
.000000E+00
.108986E-02
.550070E-02
.000000E+00
.991425E-10
.458581E-03
.686549E-04
.117031E-08
.000000E+00
.000000E+00
.725198E-02
.000000E+00
.29450E-01
```

y(i)

.540695E-02
.523952E-03
.000000E+00
.145666E-04
.000000E+00
.000000E+00
.109169E-02
.550070E-02
.000000E+00
.991425E-10
.458028E-03
.686549E-04
.117031E-08
.000000E+00
.000000E+00
.725161E-02
.000000E+00
.65785E-01

y(i)

.540695E-02
.523952E-03
.000000E+00
.145666E-04
.000000E+00
.000000E+00
.109511E-02
.550070E-02
.000000E+00
.991425E-10
.456989E-03
.686549E-04
.117031E-08
.000000E+00
.000000E+00
.725091E-02
.000000E+00

.13695

y(i)

.540695E-02
.523952E-03
.000000E+00
.145666E-04
.000000E+00
.000000E+00

.110182E-02
.550070E-02
.000000E+00
.991425E-10
.454955E-03
.686549E-04
.117031E-08
.000000E+00
.000000E+00
.724953E-02
.000000E+00
.28212
y(i)
.540695E-02
.523952E-03
.000000E+00
.145666E-04
.000000E+00
.000000E+00
.111550E-02
.550070E-02
.000000E+00
.991425E-10
.450805E-03
.686549E-04
.117031E-08
.000000E+00
.000000E+00
.724672E-02
.000000E+00
.57846

y(i)
.540695E-02
.523952E-03
.000000E+00
.145666E-04
.000000E+00
.000000E+00
.114342E-02
.550071E-02
.000000E+00
.991425E-10
.442332E-03
.686549E-04
.117031E-08

.000000E+00
.000000E+00
.724098E-02
.000000E+00
1.0000
y(i)
.540695E-02
.523952E-03
.000000E+00
.145666E-04
.000000E+00
.000000E+00
.118315E-02
.550071E-02
.000000E+00
.991425E-10
.430281E-03
.686549E-04
.117031E-08
.000000E+00
.000000E+00
.723282E-02
.000000E+00
.10099E-01
y(i)
.540795E-02
.523952E-03
.000000E+00
.145666E-04
.000000E+00
.000000E+00
.108986E-02
.550070E-02
.000000E+00
.991425E-10
.458581E-03
.686549E-04
.117031E-08
.000000E+00
.000000E+00
.725198E-02
.000000E+00
.27963E-01
y(i)
.540974E-02

.523952E-03
.000000E+00
.145666E-04
.000000E+00
.000000E+00
.109155E-02
.550070E-02
.000000E+00
.991425E-10
.458071E-03
.686549E-04
.117031E-08
.000000E+00
.000000E+00
.725164E-02
.000000E+00
.61985E-01

y(i)

.541314E-02
.523952E-03
.000000E+00
.145666E-04
.000000E+00
.000000E+00
.109475E-02
.550070E-02
.000000E+00
.991425E-10
.457098E-03
.686549E-04
.117031E-08
.000000E+00
.000000E+00
.725098E-02
.000000E+00

.12892

y(i)

.541983E-02
.523952E-03
.000000E+00
.145666E-04
.000000E+00
.000000E+00
.110106E-02
.550070E-02

.000000E+00
.991425E-10
.455184E-03
.686549E-04
.117031E-08
.000000E+00
.000000E+00
.724968E-02
.000000E+00
.26826

y(i)

.543377E-02
.523952E-03
.000000E+00
.145666E-04
.000000E+00
.000000E+00
.111419E-02
.550071E-02
.000000E+00
.991425E-10
.451201E-03
.686549E-04
.117031E-08
.000000E+00
.000000E+00
.724699E-02
.000000E+00

.55722

y(i)

.546266E-02
.523952E-03
.000000E+00
.145666E-04
.000000E+00
.000000E+00
.114142E-02
.550071E-02
.000000E+00
.991425E-10
.442940E-03
.686549E-04
.117031E-08
.000000E+00
.000000E+00

```

.724139E-02
.000000E+00
1.0000
y(i)
.550693E-02
.523951E-03
.000000E+00
.145666E-04
.000000E+00
.000000E+00
.118315E-02
.550071E-02
.000000E+00
.991426E-10
.430282E-03
.686548E-04
.117031E-08
.000000E+00
.000000E+00
.723282E-02
.000000E+00

```

\$debug

Integer n,NMAX

Parameter (NMAX=50,n=17)

Common /Param/Cio(n),dcdxo(n),z(n),D(n),Ri(n),T

Real Cio,dcdxo,D,Ri,T

Integer z

Common /Caller/x1,x2,nvar

Integer nvar

Real x1,x2

Logical check

Real dx

C n = number of species

C nvar = number of equations = 2*n

C x1 = starting point

C x2 = ending point

C dx = stepsize in diffusion layer

dx=1.0e-4

x1=0.0+dx

x2=1.0

nvar=2*n

```

$debug
  Integer n,NMAX
  Parameter (NMAX=50,n=17)
  Common /Param/Cio(n),dcdxo(n),z(n),D(n),Ri(n),T
  Real Cio,dcdxo,D,Ri,T
  Integer z,i

  Common /Caller/x1,x2,nvar
  Integer nvar
  Real x1,x2

  Logical check
  Real dx
C n = number of species
C nvar = number of equations = 2*n
C x1 = starting point
C x2 = ending point
C dx = stepsize in diffusion layer
  dx=1.0e-4
  x1=0.0+dx
  x2=1.0
  nvar=2*n

C Read in values for charge, effective diffusivity, initial concentration
C initial guess of the first derivative
  Open(Unit=1, File='datainp7.inp', Status='old')
  Open(Unit=2, File='dataout.out')
  Open(Unit=3, File='temp.inp', Status='old')
  Read(3,*) T
C   Write(2,('z(i) d(i) Cio(i) dcdxo(i) '))
  Print *,z(i) d(i) Cio(i) dcdxo(i) '
  Do i=1,17
    Read (1,*) z(i),D(i),Cio(i),dcdxo(i)
C    Write(2,*) z(i),D(i),Cio(i),dcdxo(i)
    Print*,z(i),D(i),Cio(i),dcdxo(i)
  End Do
  Close(Unit=1, Status='Keep')
  Close(Unit=3, Status='Keep')
  Call newt(dcdxo,n,check)
  Close(Unit=2, Status='keep')
  End

  Subroutine Load(x1,v,y)
  Parameter (NMAX=50,n=17)
  Real x1,v(n),y(2*n)

```

```

Common /Param/Cio(n),dcdxo(n),z(n),D(n),Ri(n),T
Real Cio,dcdxo,D,Ri,T
Integer z,k,i
Do 5 i=1,2*n,2
    k=(i+1)/2
    y(i+1)=dcdxo(k)
    y(i)=Cio(k)
5 Continue
End

```

C This subroutine calculates the sums needed for calculation of the first C and second derivatives.

```

Subroutine Sigmas(s1,s2,s3,s,y,dydx)
Parameter (NMAX=50,n=17,nvar=2*n)
Real s1,s2,s3,s(n),y(nvar),c1,c2,dydx(nvar)
Real Ea,Ec,Ecorr,alphaa,alphac,R,F,iao,ico
Real Flux(n)

```

```

Integer i,j,k

```

```

Common /Param/Cio(n),dcdxo(n),z(n),D(n),Ri(n),T
Real Cio,dcdxo,D,Ri,T
Integer z
s1=0.0
s2=0.0
s3=0.0

```

C iao and ico (mA/cm²) are found from Liu et al(1991) and Bard et al(1989)

C F is Faraday's constant in C/mol

C R is the universal gas constant in kcal/mol K

```

iao=2.00E-7
ico=4.00E-6
alphaa=0.8524474
alphac=0.9458974
R=8.314
F=96500
Ea=-0.44+(R*T/(2*F))*log(y(13))
Ec=(R*T/(2*F))*log(y(23))
Ecorr=[Ea+[(log(ico)*alphac)/(log(iao)*alphaa)]*Ec]/
# [1+(log(ico)*alphac)/(log(iao)*alphaa)]
Do 100 i=1,n
    Ri(i)=0.0
100 Continue
c Flux(11)=-52.5*exp(-5385/T)*y(16)
c Flux(14)=-9.8E6*exp(-9261/T)*y(17)
c Flux(7)=2*(Flux(11)+Flux(14))

```

```

C   print*,Flux(11),Flux(14),Flux(7)
   Ri(7)=(iao*exp((alphaa*F*(Ecorr-Ea))/(R*T)))*1.036E-8
   Ri(11)=(ico*exp((alphac*F*(Ecorr-Ec))/(R*T)))*1.036E-8
C   print*,Ri(7)
   Do 2 i=1,n,2
       k=(i+1)/2
       c1=z(k)*D(k)
       c2=z(k)*c1
       s1=s1+c1*y(i+1)
       s2=s2+c2*y(i)
       s3=s3+c2*y(i+1)
       s(i)=0.0
   Do 1 j=1,n,2
       k=(k+1)/2
       if (j.ne.k) s(i)=s(i)+z(k)*D(k)*dydx(j+1)
1       Continue
2       Continue
   Return
   End

```

C This subroutine calculates the first and second derivatives. They are stored
C in one vector. The first derivatives are stored in the odd values of (i) and
C the second derivatives are stored in the even values of (i).

```

Subroutine Derivs(x,y,dydx)
Parameter (NMAX=50,n=17)
Real y(2*n),dydx(2*n),s1,s2,s3,s(n),x(n)
Integer i,k

Common /Param/Cio(n),dcdxo(n),z(n),D(n),Ri(n),T
Integer z
call sigmas(s1,s2,s3,s,y,dydx)
C   write(2,(' dy2/dx'))
   Do 3 i=1,2*n,2
       k=(i+1)/2
C       dy1i/dx, i=odd
       dydx(i)=y(i+1)
C       dy2i/dx, i=even
       dydx(i+1)=((z(k)*s1*s3/(s2*s2))*y(i))/((1.0-z(k)*z(k)*D(k)/s2)
#           -z(k)*s(k)/s2)
C   Write(2,*) dydx(i+1)
3   Continue
   Return
   End

```

C This Subroutine calculates the function to be minimized.
Subroutine Score(x2,y,fvec)

```

Parameter(NMAX=50,n=17)
Real y(2*n),fvec(n),s1,s2,s3,s(n),ion_flux,mole_flux,
# dydx(2*n),x2
Integer i,k
Common /Param/Cio(n),dcdxo(n),z(n),D(n),Ri(n),T
Real Cio,dcdxo,D,Ri,T,del
Integer z

call sigmas(s1,s2,s3,s,y,dydx)
C   print*, 'SCORE'
    del=0.001
    Do 4 i=1,2*n,2
        k=(i+1)/2
        ion_flux=(1-(z(k)*(s1/s2)*y(i)*z(k)*D(k)))*dydx(i+1)
        #
        mole_flux=-z(k)*dydx(i)*(s1/s2)+z(k)*y(i)*s1*s3)/(s2*s2)
        mole_flux=-D(k)*y(i+1)
        fvec(k)=ion_flux + mole_flux - Ri(k)*del
4   Continue
    Return
    End

```

C.This subroutine is fdjac.for from Numerical Recipies. It evaluates the

C Jacobian for newt.for.

```

SUBROUTINE fdjac(n,x,fvec,np,df)
INTEGER n,np
REAL df(np,np),fvec(n),x(n),EPS
PARAMETER (NMAX=50,EPS=1.e-6)
CU  USES funcv
    INTEGER i,j
    REAL h,temp,f(NMAX)
    do 12 j=1,n
        temp=x(j)
        h=EPS*abs(temp)
        if(h.eq.0.)h=EPS
        x(j)=temp+h
        h=x(j)-temp
        call funcv(n,x,f)
        x(j)=temp
        write(2,('i j df(i,j)'))
    do 11 i=1,n
        df(i,j)=(f(i)-fvec(i))/h
        write(2,*)i,j,df(i,j)
11  continue
12  continue
    return

```

END

C This subroutine is fmin.for from Numerical Recipes for use with newt.for.

```
FUNCTION fmin(x)
  INTEGER n,NP
    PARAMETER (NMAX=50, NP=NMAX)
  REAL fmin,x(NMAX),fvec
  COMMON /newtv/ fvec(NP),n
  SAVE /newtv/
CU  USES funcv
  INTEGER i
  REAL sum
  call funcv(n,x,fvec)
  sum=0.
  do 11 i=1,n
    sum=sum+fvec(i)**2
11  continue
  fmin=0.5*sum
  return
END
```

C This Subroutine is Insrch.for from Numerical Recipes for use with

C newt.for.

```
SUBROUTINE Insrch(n,xold,fold,g,p,x,f,stpmax,check,func)
  INTEGER n
  LOGICAL check
  REAL f,fold,stpmax,g(n),p(n),x(n),xold(n),func,ALF,TOLX
  PARAMETER (ALF=1.e-4,TOLX=1.e-7)
  EXTERNAL func
CU  USES func (This is passed through the calling argument and is equal
C          to fmin)
  INTEGER i
  REAL a,alam,alam2,alamin,b,disc,f2,fold2,rhs1,rhs2,slope,sum,temp,
  *test,tmplam
  check=.false.
  sum=0.
  do 11 i=1,n
    sum=sum+p(i)*p(i)
11  continue
  sum=sqrt(sum)
  if(sum.gt.stpmax)then
    do 12 i=1,n
      p(i)=p(i)*stpmax/sum
12  continue
  endif
```

```

slope=0.
do 13 i=1,n
  slope=slope+g(i)*p(i)
13 continue
test=0.
do 14 i=1,n
  temp=abs(p(i))/max(abs(xold(i)),1.)
  if(temp.gt.test)test=temp
14 continue
alamin=TOLX/test
alam=1.
1 continue
do 15 i=1,n
  x(i)=xold(i)+alam*p(i)
15 continue
f=func(x)
if(alam.lt.alamin)then
do 16 i=1,n
  x(i)=xold(i)
16 continue
check=.true.
return
else if(f.le.fold+ALF*alam*slope)then
  return
else
  if(alam.eq.1.)then
    tmlam=-slope/(2.*(f-fold-slope))
  else
    rhs1=f-fold-alam*slope

    rhs2=f2-fold2-alam2*slope
    a=(rhs1/alam**2-rhs2/alam2**2)/(alam-alam2)
    b=(-alam2*rhs1/alam**2+alam*rhs2/alam2**2)/(alam-alam2)
    if(a.eq.0.)then
      tmlam=-slope/(2.*b)
    else
      disc=b*b-3.*a*slope
      if(disc.lt.0.) pause 'roundoff problem in lnsrch'
      tmlam=(-b+sqrt(disc))/(3.*a)
    endif
    if(tmlam.gt..5*alam)tmlam=.5*alam
  endif
endif
alam2=alam

```



```

f2=f
fold2=fold
alam=max(tmplam,.1*alam)
goto 1
END

```

C This Subroutine is lubksb.for from Numerical Recipies for use with newt.for.

```

SUBROUTINE lubksb(a,n,np,indx,b)
INTEGER n,np,indx(n)
REAL a(np,np),b(n)
INTEGER i,ii,j,ll
REAL sum
ii=0
do 12 i=1,n
  ll=indx(i)
  sum=b(ll)
  b(ll)=b(i)
  if (ii.ne.0)then
    do 11 j=ii,i-1
      sum=sum-a(i,j)*b(j)
11.  continue
    else if (sum.ne.0.) then
      ii=i
    endif
  b(i)=sum
12. continue
do 14 i=n,1,-1
  sum=b(i)
  do 13 j=i+1,n
    sum=sum-a(i,j)*b(j)
13.  continue
  b(i)=sum/a(i,i)
14. continue
return
END

```

C This Subroutine is ludcmp.for from Numerical Recipies for use with newt.for

```

SUBROUTINE ludcmp(a,n,np,indx,d)
INTEGER n,np,indx(n),NMAX
REAL d,a(np,np),TINY
PARAMETER (NMAX=50,TINY=1.0e-30)
INTEGER i,imax,j,k
REAL aamax,dum,sum,vv(NMAX)
d=1.

```

```

do 12 i=1,n
  aamax=0.
  do 11 j=1,n
    if (abs(a(i,j)).gt.aamax) aamax=abs(a(i,j))
11  continue
  if (aamax.eq.0.) pause 'singular matrix in ludcmp'
  vv(i)=1./aamax
12  continue
  do 19 j=1,n
    do 14 i=1,j-1
      sum=a(i,j)
      do 13 k=1,i-1
        sum=sum-a(i,k)*a(k,j)
13  continue
      a(i,j)=sum
14  continue
    aamax=0.
    do 16 i=j,n

      sum=a(i,j)
      do 15 k=1,j-1
        sum=sum-a(i,k)*a(k,j)
15  continue
      a(i,j)=sum
      dum=vv(i)*abs(sum)
      if (dum.ge.aamax) then
        imax=i
        aamax=dum
      endif
16  continue
    if (j.ne.imax)then
      do 17 k=1,n
        dum=a(imax,k)
        a(imax,k)=a(j,k)
        a(j,k)=dum
17  continue
      d=-d
      vv(imax)=vv(j)
    endif
    indx(j)=imax
    if(a(j,j).eq.0.)a(j,j)=TINY
    if(j.ne.n)then
      dum=1./a(j,j)

      do 18 i=j+1,n

```

```

    a(i,j)=a(i,j)*dum
18  continue
    endif
19  continue
    return
    END

```

C This subroutine is newt.for from Numerical Recipes. It is a globally
C convergent Newton-Raphson routine.

```

    SUBROUTINE newt(x,n,check)
    INTEGER n,nn,NP,MAXITS
    LOGICAL check
    REAL x(n),fvec,TOLF,TOLMIN,TOLX,STPMX
    PARAMETER (NMAX=50,NP=NMAX,MAXITS=200,TOLF=1.e-4,TOLMIN=1.e-
6,
    *TOLX=1.e-7,STPMX=100.)
    COMMON /newtv/ fvec(NP),nn
    SAVE /newtv/
CU  USES fdjac,fmin,lnsrch,lubksb,ludcmp
    INTEGER i,its,j,indx(NP)
    REAL d,den,f,fold,stpmax,sum,temp,test,fjac(NP,NP),g(NP),p(NP),
*xold(NP),fmin
    EXTERNAL fmin
    nn=n
    f=fmin(x)
    test=0.
    do 11 i=1,n
        if(abs(fvec(i)).gt.test)test=abs(fvec(i))
11  continue
        if(test.lt..01*TOLF)then
            check=.false.
            return
        endif
        sum=0.
        do 12 i=1,n
            sum=sum+x(i)**2
12  continue
        stpmax=STPMX*max(sqrt(sum),float(n))
        do 21 its=1,MAXITS
            call fdjac(n,x,fvec,NP,fjac)
            do 14 i=1,n
                sum=0.
                do 13 j=1,n
                    sum=sum+fjac(j,i)*fvec(j)

```

```

13  continue
    g(i)=sum
14  continue
    do 15 i=1,n
        xold(i)=x(i)
15  continue
    fold=f
    do 16 i=1,n
        p(i)=-fvec(i)
16  continue
    call ludcmp(fjac,n,NP,indx,d)
    call lubksb(fjac,n,NP,indx,p)
    call lnsrch(n,xold,fold,g,p,x,f,stpmax,check,fmin)
    test=0.

    do 17 i=1,n
        if(abs(fvec(i)).gt.test)test=abs(fvec(i))
17  continue
    if(test.lt.TOLF)then
        check=.false.
        return
    endif
    if(check)then
        test=0.
        den=max(f,.5*n)
        do 18 i=1,n
            temp=abs(g(i))*max(abs(x(i)),1.)/den
            if(temp.gt.test)test=temp
18  continue
        if(test.lt.TOLMIN)then
            check=.true.
        else
            check=.false.
        endif
        return
    endif
    test=0.
    do 19 i=1,n
        temp=(abs(x(i)-xold(i)))/max(abs(x(i)),1.)
        if(temp.gt.test)test=temp
19  continue
    if(test.lt.TOLX)return

21  continue
    pause 'MAXITS exceeded in newt'

```

END

```
C   odeint.for
SUBROUTINE odeint(ystart,nvar,x1,x2,eps,h1,hmin,nok,nbad,derivs,
*rkqs)
INTEGER nbad,nok,nvar,KMAXX,MAXSTP,NMAX
REAL eps,h1,hmin,x1,x2,ystart(nvar),TINY
EXTERNAL derivs,rkqs
PARAMETER (MAXSTP=10000,NMAX=50,KMAXX=200,TINY=1.e-30)
INTEGER i,kmax,kount,nstp
REAL dxsav,h,hdid,hnext,x,xsav,dydx(NMAX),xp(KMAXX),y(NMAX),
*yp(NMAX,KMAXX),yscal(NMAX)
COMMON /path/ kmax,kount,dxsav,xp,yp
x=x1
h=sign(h1,x2-x1)
nok=0
nbad=0
kount=0
do 11 i=1,nvar

    y(i)=ystart(i)
11  continue
    if (kmax.gt.0) xsav=x-2.*dxsav
    do 16 nstp=1,MAXSTP
        call derivs(x,y,dydx)
        do 12 i=1,nvar
            yscal(i)=abs(y(i))+abs(h*dydx(i))+TINY
12  continue
        if(kmax.gt.0)then
            if(abs(x-xsav).gt.abs(dxsav)) then
                if(kount.lt.kmax-1)then
                    kount=kount+1
                    xp(kount)=x
                    do 13 i=1,nvar
                        yp(i,kount)=y(i)
13  continue
                    xsav=x
                endif
            endif
        endif
        if((x+h-x2)*(x+h-x1).gt.0.) h=x2-x

    call rkqs(y,dydx,nvar,x,h,eps,yscal,hdid,hnext,derivs)
    if(hdid.eq.h)then
        nok=nok+1
```

```

else
  nbad=nbad+1
endif
if((x-x2)*(x2-x1).ge.0.)then
  do 14 i=1,nvar
    ystart(i)=y(i)
14  continue
    if(kmax.ne.0)then
      kount=kount+1
      xp(kount)=x
      do 15 i=1,nvar
        yp(i,kount)=y(i)
15  continue
      endif
      return
    endif
    if(abs(hnext).lt.hmin) pause
    *'stepsize smaller than minimum in odeint'

    h=hnext
16  continue
    pause `too many steps in odeint'
    return
  END

```

C This subroutine is rkqs.for from Numerical Recipes for use with newt.for.

C It is a fifth order Runge-Kutta method.

```

SUBROUTINE rkqs(y,dydx,n,x,htry,eps,yscal,hdid,hnext,derivs)
  INTEGER n,NMAX
  REAL eps,hdid,hnext,htry,x,dydx(n),y(n),yscal(n)
  EXTERNAL derivs
  PARAMETER (NMAX=50)
CU  USES derivs,rkck
  INTEGER i
  REAL errmax,h,htemp,xnew,yerr(NMAX),ytemp(NMAX),SAFETY,PGROW,
  *PSHRNK,ERRCON
  PARAMETER (SAFETY=0.9,PGROW=-.2,PSHRNK=-.25,ERRCON=1.89e-4)
  h=htry
1  call rkck(y,dydx,n,x,h,ytemp,yerr,derivs)
  errmax=0.
  do 11 i=1,n
    errmax=max(errmax,abs(yerr(i)/yscal(i)))
11  continue
  errmax=errmax/eps
  if(errmax.gt.1.)then

```

```

htemp=SAFETY*h*(errmax**PSHRNK)

h=sign(max(abs(htemp),0.1*abs(h)),h)
xnew=x+h
if(xnew.eq.x)pause 'stepsize underflow in rkqs'
goto 1
else
if(errmax.gt.ERRCON)then
hnext=SAFETY*h*(errmax**PGROW)
else
hnext=5.*h
endif
hdid=h
C Increment x here for the next stepsize.
x=x+h
do 12 i=1,n
y(i)=ytemp(i)
write(2,('y(i)'))
write(2,*) i,y(i)
12 continue

return
endif
END

C This Subroutine is for use with rkqs.for from Numerical Recipes.
SUBROUTINE rkck(y,dydx,n,x,h,yout,yerr,derivs)
INTEGER n,NMAX
REAL h,x,dydx(n),y(n),yerr(n),yout(n)
EXTERNAL derivs
PARAMETER (NMAX=50)
CU USES derivs
INTEGER i
REAL ak2(NMAX),ak3(NMAX),ak4(NMAX),ak5(NMAX),ak6(NMAX),
*ytemp(NMAX),A2,A3,A4,A5,A6,B21,B31,B32,B41,B42,B43,B51,B52,B53,
*B54,B61,B62,B63,B64,B65,C1,C3,C4,C6,DC1,DC3,DC4,DC5,DC6
PARAMETER (A2=.2,A3=.3,A4=.6,A5=1.,A6=.875,B21=.2,B31=3./40.,
*B32=9./40.,B41=.3,B42=-.9,B43=1.2,B51=-11./54.,B52=2.5,

*B53=-70./27.,B54=35./27.,B61=1631./55296.,B62=175./512.,
*B63=575./13824.,B64=44275./110592.,B65=253./4096.,C1=37./378.,
*C3=250./621.,C4=125./594.,C6=512./1771.,DC1=C1-2825./27648.,
*DC3=C3-18575./48384.,DC4=C4-13525./55296.,DC5=-277./14336.,
*DC6=C6-.25)
do 11 i=1,n

```

```

    ytemp(i)=y(i)+B21*h*dydx(i)
11  continue
    call derivs(x+A2*h,ytemp,ak2)
    do 12 i=1,n
        ytemp(i)=y(i)+h*(B31*dydx(i)+B32*ak2(i))
12  continue
    call derivs(x+A3*h,ytemp,ak3)
    do 13 i=1,n
        ytemp(i)=y(i)+h*(B41*dydx(i)+B42*ak2(i)+B43*ak3(i))

13  continue
    call derivs(x+A4*h,ytemp,ak4)
    do 14 i=1,n
        ytemp(i)=y(i)+h*(B51*dydx(i)+B52*ak2(i)+B53*ak3(i)+B54*ak4(i))
14  continue
    call derivs(x+A5*h,ytemp,ak5)
    do 15 i=1,n
        ytemp(i)=y(i)+h*(B61*dydx(i)+B62*ak2(i)+B63*ak3(i)+B64*ak4(i)+
        *B65*ak5(i))
15  continue
    call derivs(x+A6*h,ytemp,ak6)
    do 16 i=1,n
        yout(i)=y(i)+h*(C1*dydx(i)+C3*ak3(i)+C4*ak4(i)+C6*ak6(i))
        write(2,("yout(i)"))
        write(2,*) yout(i)
16  continue
    do 17 i=1,n
        yerr(i)=h*(DC1*dydx(i)+DC3*ak3(i)+DC4*ak4(i)+DC5*ak5(i)+DC6*
        *ak6(i))
        write(2,("yerr(i)"))
        write(2,*) yerr(i)
17  continue
    return
    END

```

C shoot.for

```

CU  SUBROUTINE shoot(n2,v,f) is named "funcv" for use with "newt"
    SUBROUTINE funcv(n2,v,f)
        INTEGER n2,nvar,kmax,kount,KMAXX,NMAX
        REAL f(n2),v(n2),x1,x2,dxsav,yp,eps
        PARAMETER (NMAX=50,KMAXX=200,eps=1.e-6)
        COMMON /caller/ x1,x2,nvar
        COMMON /path/ kmax,kount,dxsav,yp(KMAXX),yp(NMAX,KMAXX)
CU  USES derivs,load,odeint,rkqs,score
    INTEGER nbad,nok

```



```
REAL h1,hmin,y(NMAX)
EXTERNAL derivs,rkqs
kmax=0
h1=(x2-x1)/100.
hmin=0.

      call load(x1,v,y)
call odeint(y,nvar,x1,x2,EPS,h1,hmin,nok,nbad,derivs,rkqs)
call score(x2,y,f)

return
END
```

VITA ²

Shannon Dugan

Candidate for the Degree of

Master of Science

Thesis: A MATHEMATICAL MODEL FOR CALCULATING MASS TRANSFER IN THE DIFFUSION LAYER

Major Field: Chemical Engineering

Biographical:

Personal Data: Born in Tulsa, Oklahoma on September 27, 1972, the daughter of Sally Buttler, the wife of Brian E. Dugan.

Education: Graduated from Owasso High School, Owasso, Oklahoma in May 1990; received Bachelor of Science degree in Chemistry from Oklahoma State University, Stillwater, Oklahoma in May 1995. Completed the requirements for the Master of Science degree with a major in Chemical Engineering at Oklahoma State University in December, 1998

Experience Employed as holiday sales/cashier for Eddie Bauer clothing company; interned for Hoechst Celanese in the summer of 1996; employed by Oklahoma State University Department of Chemistry as an undergraduate and graduate research assistant and graduate teaching assistant 1994 to 1996; employed by Oklahoma State University School of Chemical Engineering as a graduate teaching and research assistant 1996 to 1997

Professional Memberships: American Institute of Chemical Engineers, American Chemical Society